2007

Nanomaterials for Organic Solar Cells

Annick Anctil

Nanomaterials for Organic Solar Cells

Annick Anctil

August, 2007
Thesis

Submitted in Partial Fulfillment of the Requirements for the Degree of Master of Science

Approved:

Ryne P. Raffaelle
Thesis Advisor, Dr. Ryne P. Raffaelle

Department of Materials Science and Engineering
Rochester Institute of Technology
Rochester, New York 14623

Thesis/Dissertation Author Permission Statement

Title of thesis or dissertation: Nanomaterials for Organic Solar Cells

Name of author: Annick Anctil
Degree: Master
Program: Materials Science and Engineering
College: Science

I understand that I must submit a print copy of my thesis or dissertation to the RIT Archives, per current RIT guidelines for the completion of my degree. I hereby grant to the Rochester Institute of Technology and its agents the non-exclusive license to archive and make accessible my thesis or dissertation in whole or in part in all forms of media in perpetuity. I retain all other ownership rights to the copyright of the thesis or dissertation. I also retain the right to use in future works (such as articles or books) all or part of this thesis or dissertation.

Print Reproduction Permission Granted:

I, Annick Anctil, hereby **grant permission** to the Rochester Institute Technology to reproduce my print thesis or dissertation in whole or in part. Any reproduction will not be for commercial use or profit.

Signature of Author: Annick Anctil Date: _____

Print Reproduction Permission Denied:

I, _____, hereby **deny permission** to the RIT Library of the Rochester Institute of Technology to reproduce my print thesis or dissertation in whole or in part.

Signature of Author: _____ Date: _____

Inclusion in the RIT Digital Media Library Electronic Thesis & Dissertation (ETD) Archive

I, _____, additionally grant to the Rochester Institute of Technology Digital Media Library (RIT DML) the non-exclusive license to archive and provide electronic access to my thesis or dissertation in whole or in part in all forms of media in perpetuity.

I understand that my work, in addition to its bibliographic record and abstract, will be available to the world-wide community of scholars and researchers through the RIT DML. I retain all other ownership rights to the copyright of the thesis or dissertation. I also retain the right to use in future works (such as articles or books) all or part of this thesis or dissertation. I am aware that the Rochester Institute of Technology does not require registration of copyright for ETDs.

I hereby certify that, if appropriate, I have obtained and attached written permission statements from the owners of each third party copyrighted matter to be included in my thesis or dissertation. I certify that the version I submitted is the same as that approved by my committee.

Signature of Author: _____ Date: _____

Abstract

Organic solar cells performances are mainly limited by photon absorption due to the mismatch between the conducting polymer and the solar spectrum, as well as, exciton diffusion since the excitons are not efficiently dissociated into free charges. Nanomaterials such as fullerenes, quantum dots, and carbon nanotubes were investigated in combination with conjugated polymers to allow for a broader harvesting of the solar spectrum. For P3HT:PCBM solar cells, optimal efficiencies were obtained using a combination of annealing before, as well as, after contact deposition. Using the concepts developed for P3HT, the effect of solvent, molecular weight, and the type of fullerenes was investigated using MEH-PPV. Efficiencies were increased from 0.57% to 2.06% under AM1.5 by optimizing the polymer molecular weight, the device thickness and the fullerene derivative. Three types of quantum dots were investigated to enhance photoconversion below the polymer absorption: CdSe, InP and InAs QDs. Sub-bandgap photoconversion was observed around 1.3 eV for InAs QDs. Finally, both SWNT and WMNT were investigated for improved charge dissociation and transport in organic solar cells. The maximum loading of carbon nanotubes was increased by using cut carbon nanotubes as well as by using an intrinsic layer. The most promising option for using carbon nanotubes in polymeric solar cells was found to be the MWNT aligned arrays.

Table of Contents

List of Figures

Chapter 1: Introduction

Currently there exists a large need for inexpensive renewable energy sources; particularly low-cost photovoltaic devices. For this reason, organic solar cells have been receiving an increasing amount of attention over the last decade. These devices offer the potential for low cost processing, flexibility, and light weight that could meet the needs of a number of applications. Not only are organic semiconductors cheaper than their inorganic counterparts, but due to the means by which they are fabricated, their properties can be controlled during chemical synthesis.

Organic semiconductor development started in the 1970s, but the interest in these materials increased dramatically after Tang created the first homojunction in 1986.[1] However, a major milestone in organic photovoltaics was achieved by Yu et al. in 1995 in which both electron donor and acceptor materials were blended into a single layer and created what is now called a bulk heterojunction.[2] Blending had the advantage of increasing the interfacial area between the donor and acceptor, resulting in considerably higher photocurrent density. Recently efficiencies up to 5% have been reported by optimizing the nanomorphology of these heterojunctions using fullerenes derivatives in particular in combination with conjugated polymers.[3, 4] In order to get a better understanding of the limitations and current challenges of organic solar cells, it is essential to understand the photogeneration process in a typical bulk heterojunction as illustrated in Figure 1.

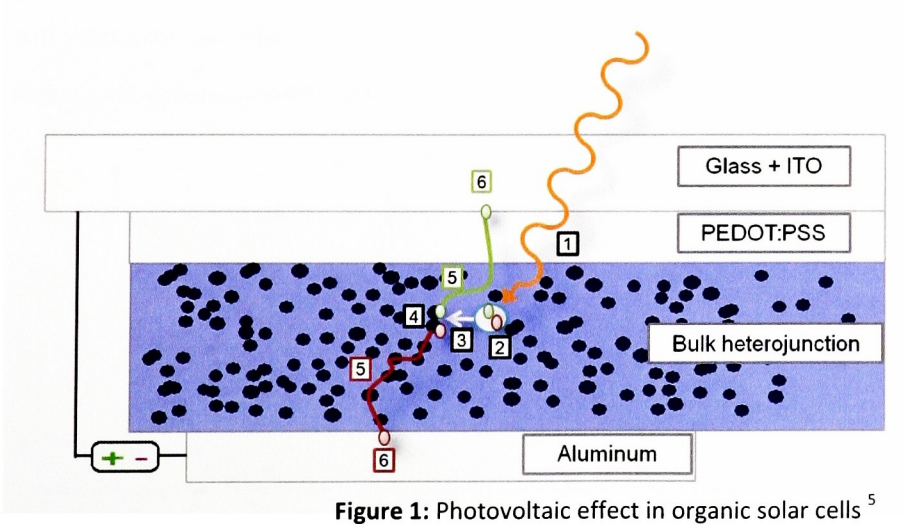

Figure 1: Photovoltaic effect in organic solar cells [5]

According to Figure 1, an exciton is first generated during photon absorption due to the electronic transition from HOMO to LUMO levels in the donor material. Photon absorption depends on the optical absorption coefficient as well as the thickness of the donor material. This photoexcitation results in the generation of an electron-hole pair which is in an excited but neutral state with limited lifetime. The electron and the hole are bound by an energy which is smaller than the energy gap between the permitted bands and form what is called an exciton. The exciton binding energy is around 0.1 to 0.2 eV for organic materials.[6] Due to its limited lifetime, the exciton needs to diffuse fast enough to a junction before recombination can take place in order to contribute to the photocurrent. This limited diffusion length severely limits the thickness of these devices. In the presence of a sufficiently strong internal electric field, the exciton can split into a free hole and an electron. This internal field can be provided at the donor-acceptor interface, if the difference in electron affinities is suitable. It is estimated that only 10% of photoexcitations lead to free charge carriers in conjugated polymers.[7] Blending of conjugated polymers with electron acceptors such as fullerenes, is a very efficient way to break apart photoexcited excitons into free charge carriers. Once the charges are free, they travel towards the electrodes using the classic hopping mechanism in organic materials.[8] However, their mobility can be reduced by traps.

A gradient in the chemical potentials of electrons and holes is built up in a donor-acceptor junction which is determined by the difference between the HOMO level of the donor and the LUMO levels of the acceptor.[7] This internal electrical field determines the maximum open circuit voltage (Voc) and contributes to the field-induced drift of charge carriers. Finally, the charges can be collected at the electrodes as long as: $(E_f)_{cathode}<(E_{LUMO})_{acceptor}$ and $(E_f)_{anode}>(E_{HOMO})_{donor}$ (see Figure 2).

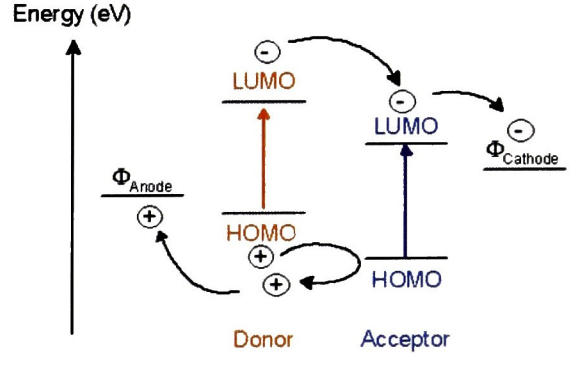

Figure 2: Conditions for charge transfer

In order to obtain an efficient solar cell, all the steps discussed above have to be optimized. First, to optimize the photon absorption, the optical losses have to be minimized. Considering that the refractive index of organic materials is relatively low, the reflection coefficient is also relatively low (~4%)[6] and therefore is not the main factor. The poor photon absorption is mainly due to the mismatch between the solar spectrum and the absorption spectrum of the conducting polymer. In theory, to have an optimal solar cell, the acceptor bandgap should be around 1.4 eV for which the maximum efficiency would be 31 % under 1 sun AM1.5.[9] The majority of semiconducting polymers have bandgaps higher than 2 eV (620 nm), which limits the possible theoretical maximum photovoltaic conversion efficiency to less than 30%.[10]

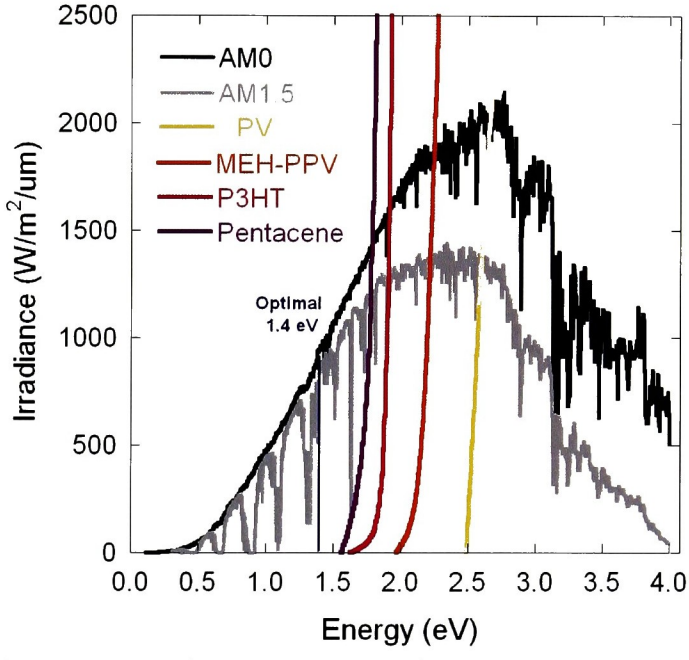

Figure 3: AMO and AM1.5 spectrum with various polymer absorption

Photon absorption can also be maximized by optimizing the device thickness. A sample too thin causes part of the incident radiation to be unabsorbed, resulting in these photons not contributing to the charge generation. Conversely, a sample too thick causes series resistance due to the exciton generation zone being too far from an interface. Subsequently, recombination occurs before dissociation of the excitons. Since polymer absorptions coefficients may reach $10^5 cm^{-1}$, a 100 nm thickness is generally enough to absorb most of the photons.[7]

Another main challenge is related to the exciton diffusion due to conjugated polymers, which exhibit poor charge transport in bulk heterojunctions. In order to increase the efficiency, the donor and acceptor phases should be separated by a distance of 10 to 20 nm and the interfacial area should be increased. The use of different work-function electrodes, as well as concentration gradients, can contribute to the charge transport toward the electrodes. The donor and acceptor phases must form an interpenetrating network to efficiently dissociate and transport the charges. This nanoscale morphology has been shown to be strongly affected by the processing conditions, such as the deposition technique, the solvent, the processing temperatures, the donor/acceptor ratio, the solution concentration, and the thermal annealing.

Therefore, to improve efficiency, an improved harvesting of light could be achieved through the use of various nanomaterials which will contribute through energy-transfer. The focus of this dissertation will be on the investigation of nanomaterials including fullerenes, quantum dots, and carbon nanotubes to determine these effects on the production of energy in various conjugated polymers solar cells. Since the morphology of the active layer has a direct impact on the performance of the organic solar cells, various processing studies will also be presented (solvent, annealing, components ratio, molecular weight). With this objective in mind, the various materials that were studied are described below.

1.1 Conjugated Polymers

The conjugated polymers backbone is composed of alternating single and double bonds. Each carbon binds only to three adjacent atoms, resulting in one electron per carbon left in the P_z orbital. The overlap of these P_z orbitals causes the formation of π bonds along the backbone, and delocalization of the π electrons. Polymers with a delocalized π electron system can absorb sunlight, create photogenerated charge carriers and transport these charge carriers. The absorption of conjugated polymers ranges from yellow to red. The absorption for one type of polymer can also be changed by the addition of various pending groups.[11]

The principal conjugated polymers can be divided in 3 families[7] :

I. Derivatives of phenylene vinylene backbones (poly[2-methoxy-5-(3,7-dimethyloctyloxy)]-1,4-phenylevinylene (MEH-PPV)

II. Derivatives of thiophenes chains (poly(3-hexylthiophene) (P3HT)

III. Derivatives of fluorine backbones (poly(9,9'-dioctylfluorene-co-bis-N,N'-(4-butylphenyl-1,4-phenylenediamine) PFB

The two principal conjugated polymers investigated for this project were Poly[2-methoxy-5-(2-ethylhexyloxy)-1,4-phenylenevinylene] (MEH-PPV) and (Poly(3-hexylthiophene-2,5-diyl)) (P3HT)

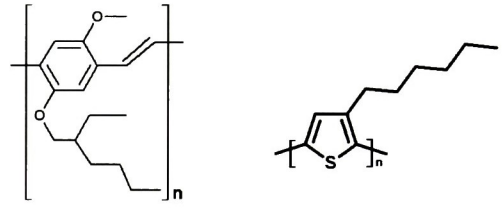

Figure 4: Chemical structures of MEH-PPV and P3HT

The poly(3-alkyls) (P3AT) family of polymer is comprised of derivatives of thiophenes with different regioregularity and pending chains. All polythiophenes have similar optical bandgaps in the order of 1.9 eV. As the chain length is increased, the electrochemical bandgap also increases. P3AT are polythiophenes with three asymmetric substituted thiophenes, resulting in 3 possible couplings between the 2 and 5 positions. The head-head configuration (HH:2-2 coupling) causes the thiophene group to be out of phase, which reduces the conjugation and the conductivity of the polymer.

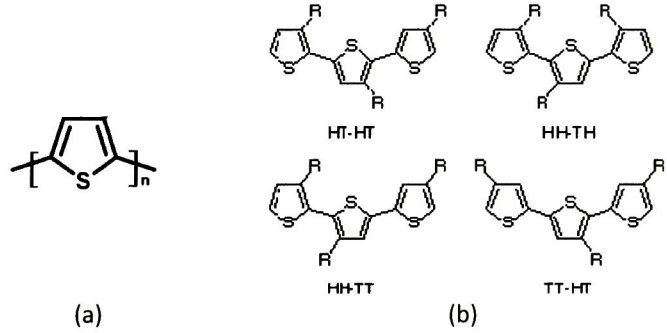

Figure 5: (a) Polythiophene and (b) the 4 possible triads resulting from combination of the 3 possible diads[12]

The record power efficiency devices have been fabricated using poly(3-hexylthiophene) with high regioregularity. High regioregularity optimizes the chain packing, which improves the optical and transport properties of the P3HT:PCBM blend upon annealing.[13] Microcrystalline lamellar stacking is generally accepted as the main factor for high efficiency devices. This structure can be improved through thermal annealing[14] and combined thermal and external voltage annealing.[15,16] The optimal annealing temperature is related to the glass transition temperature which varies with molecular weight and polydispersity. Annealing causes recrystalization, resulting in improved charge transfer and a reduced density of defects at the interfaces.[7]

Poly(p-phenylene vinylene) (PPV) is a conductive polymer with limited interest for organic solar cells due to its absorption around 2.5 eV. By modifying this basic structure to poly[2-methoxy-5-(3,7-dimethyloctyloxy)]-1,4-phenylevinylene (MEH-PPV), the band gap has shifted to lower energy (~2.1 eV), which is an improved energy absorption for the solar spectrum.

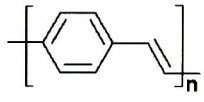

Poly(p-phenylene vinylene)
PPV

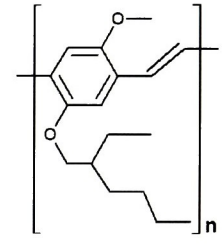

Poly[2-((2-ethylhexyl)oxy-5-methoxy-*p*-phenylene)vinylene]
MEH-PPV

Figure 6: Chemical structure of PPV and MEH-PPV

The addition of branched side chains also improves the solubility of the derivative compared to PPV that allows solution processing and easy blending of polymers for the preparation of bulk heterojunction.[11] The hole-conductivity for MEH-PPV is lower than P3HT. In order to obtain an efficient charge separation, a 4:1 (PCBM: MEH-PPV) weight ratio is typically used. Due to the high efficiencies obtained with P3HT, MEH-PPV has not been a focus of research. However with an open-circuit voltage of approximately 0.8V, compared to 0.6V for bulk heterojunctions with C60PCBM, MEH-PPV represents an interesting alternative for increasing efficiencies. At this point, the highest efficiency reported is 2.07% under AM1.5 (80 mW/cm^2) with a fill factor of 44.4%.[17] Compared to P3HT, only little investigation on the

annealing and optimal processing conditions has been done and this has resulted in lower efficiencies for this polymer-fullerene system.

1.2 Fullerene Derivatives

Carbon fullerene typically refers to a molecule containing 60 carbon atoms with icosahedral symmetry. It also includes larger molecular weight fullerenes such as C70, C76, C78 C80 that possess different geometric structures[18] .

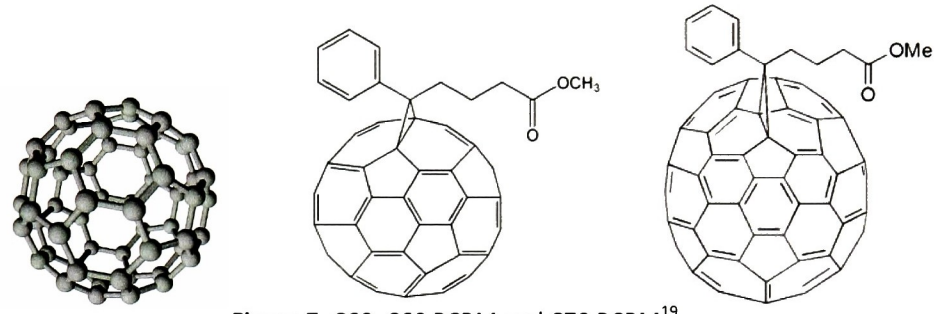

Figure 7: C60, C60 PCBM and C70 PCBM[19]

C60 or buckminsterfullerene, is an electron acceptor that can be electrochemically reduced up to 6 electrons. Its solubility is limited, therefore a soluble derivative called PCBM (1-(3-methoxycarbonyl)propyl-1-phenyl[6,6]C61) which was first synthesized by Wuld et al., is mainly used to make solar cells[7].

The size and dispersion of the PCBM nanophases have a direct impact on the devices' performances. The most widely used composition ratio of PCBM:P3HT is 1:1. For this ratio, a sudden drop in efficiency is observed after short annealing; an effect associated to the formation of large PCBM aggregates. By lowering the PCBM:P3HT ratio to 0.8:1, the annealing temperature has been increased from 110°C to 150°C, resulting in higher efficiencies. The higher annealing temperature improves the recrystalization. The lower PCBM content reduce the size of the PCBM aggregates causing degradation, allowing longer annealing time. Since the structure is closer to a equilibrium mixture, degradation of the completed device is also slower.[3] Only recently has this ratio been reduced further to 0.6:1 making the first 6% efficient device reported.[14]

1.3 Quantum Dots

Generally, polymer photovoltaic devices rely solely on photon absorption by the conducting polymer and are bandgap limited (typically > 2 eV) in regards to the solar spectrum. Quantum dots are capable of size-dependent optical absorption, exciton dissociation centers in conjugated polymers, and a means for carrier transport. Therefore, the combination of organic and inorganic semiconductors offer the possibility of absorbing a larger portion of the solar spectrum. By varying the size and the material of the quantum dots, the band gap can be tuned to the desired range.

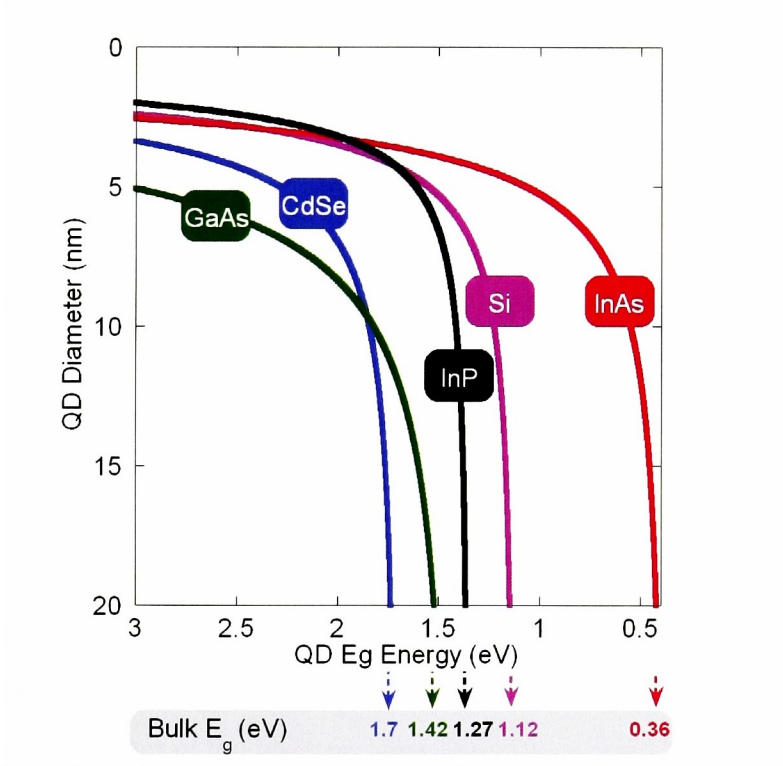

Figure 8: Bandgap tuning with particle size for various semi-conductors

Using QDs is considered a promising option since inorganic semiconductor nanoparticles can have high absorption coefficients and high photoconductivity compared to many organic semiconductor materials. Excitons which are created upon photo-excitation are separated into free charges efficiently at interfaces between organic semiconductors and inorganic semiconductors. Hybrid solar cells have been demonstrated in conjugated polymer blends containing CdSe, $CuInS_2$, CdS and PbS.[7]

Compared to dye molecules, appropriately synthesized semiconductor QDs offer wider tunability with narrower and more stable fluorescence. QDs are also particularly suited for the near-IR region where the increased absorption is needed because organic dyes have poor emission efficiency in that region.[20]

The synthesis of colloidal nanocrystals is a special case of crystallization that yields massive number of crystals in solution with identical dimensions. The interest in QDs started in the 1980s, but the first real success in their production was obtained using an organometallic approach in coordinating solvent in the early 1990s.[21] This approach originated from the utilization of organometallic compounds in the formation of extremely high quality quantum wells through metal organic chemical vapor deposition (MOCVD) methods. Organometallic reactions are extremely sensitive to air and moisture due to high reactivity of the precursors. The coordinating solvents are used to balance the reactivity of the precursors.[22] To obtain high quality crystalline QDs, it is generally established that high temperature is required.

To date, most of the research on QDs for solar cell composites has focused on CdSe since their synthesis is relatively straightforward and allows narrow distribution of QDs with specific absorption. Other researchers have tried to fabricate composite devices using MEH-PPV or P3HT. Their low efficiencies (<0.05%) can be mostly attributed to device fabrication.[23,24] In order to develop a general method for device preparation and characterization, CdSe QDs has been investigated in combination with MEH-PPV. However, since the absorption of these QD is similar to the polymer bandgap, only a relatively minor improvement by comparison to the pure polymer can be expected.

A greater improvement of the photovoltaic performance could be achieved through the use of III-V QDs, which have the appropriate bandgap in the desired absorption. The quality of QDs for III-V semiconductors as well as their synthesis have not reached the same level as the CdSe. Indium phosphide QDs was the first III-V system to be synthesized through non-covalent approaches. However, this system is extremely sensitive to air and moisture as well as to the fatty acids' chain length. The non-coordinating approach has been studied thoroughly by various groups for InP, but only by Battaglia et al. for InAs.[25] Organometallic approaches in coordinating solvents for InAs are still the most widely used, but due to their high reactivity and

extreme toxicity, a special handling precaution has to be taken.[22] Although the viability of QD-based polymer solar cells has been described in the literature, InAs QDs have only recently been shown to exhibit a photoresponse in conjunction with nanocrystalline TiO_2 films.[26] InP and InAs QDs will be investigated in organic solar cells. Due to the absorption peak of InAs, a sub-gap conversion may occur.

1.4 Carbon Nanotubes

Due to their unique properties, carbon nanotubes can be envisaged for various roles in photovoltaic devices. Single wall carbon nanotubes (SWNT) have received, so far, the most interest due to their semi-conducting properties. SWNT's have been used as electron acceptor and electron extracting electrode in bulk heterojunctions.[27] Multi-wall carbon nanotubes have been used as the hole-extracting electrode, which has resulted in a reduction of series resistance and an increase in fill factor.[28]

Growth of aligned arrays of carbon nanotubes on ITO may also be used as three-dimensional hole collecting electrodes. Bulk heterojunctions have partially resolved the issue of the short exciton diffusion length in organic PV, however, the low charge mobility of conjugated polymers remains a limiting effect. This low charge mobility may be improved by the interpenetrating electrode, which extracts the charges more efficiently. Only recently have aligned arrays of carbon nanotubes been used as large electrodes for organic photovoltaic.[28]

Chapter 2: Fullerenes

2.1 Experimental

Two types of fullerenes derivatives, C60 PCBM and C70 PCBM, were investigated as electron acceptors in bulk heterojunction. Bulk heterojunction nanostructures have a direct influence on device performance. For this reason, the effect of spin-speed, the type of solvent, annealing (pre-post annealing), PCBM ratio and polymer molecular weight has been studied for MEH-PPV and P3HT.

Bulk heterojunction solar cells were fabricated following the sandwich structure ITO/PEDOT:PSS/Active layer/Al illustrated in Figure 9. The glass substrate is coated with indium tin oxide (ITO) (Delta 7-10 Ω/sq), which is cleaned using a 2 stage ultrasonic cleaning procedure with acetone and isopropanol and dried.

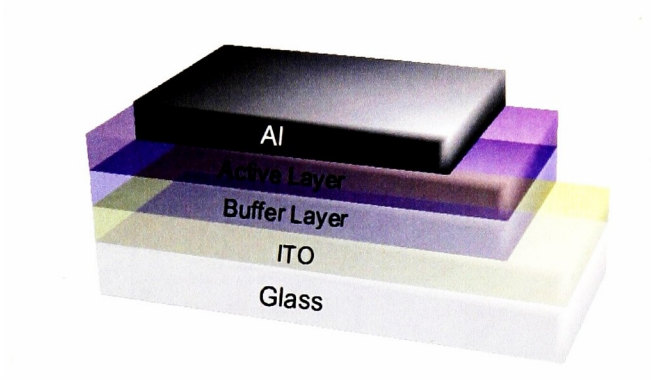

Figure 9: Schematic layout of a bulk heterojunction

Poly(ethylene-dioxythiophene) doped with polystyrene-sulfonic acid (PEDOT:PSS) was then spin-coated at 3500-4500 rpm to obtain a thickness layer around 60 to 80 nm. The PEDOT:PSS layer improved the surface quality as well as facilitated the hole injection/extraction. It is necessary to dry the Pedot:PSS layer at 110°C for 1 hour to remove any water and reduce future degradation.[7]

The active layer components are sonicated and mixed in the appropriate solvent (DCB for P3HT and *o*-xylene for MEH-PPV) before spin-coating on top of the PEDOT:PSS layer. Drying and annealing was performed inside an oven filled with argon to prevent

device degradation. For selected studies, post-annealing was performed on completed devices in a glovebox using a hot plate. The back electrical contact was 1000 Å of evaporated aluminum and the active area was calculated for current density measurement.

The current-voltage curves were obtained using a Keithley 237 source-measure unit and a Newport Oriel Instrument light source, calibrated under air mass 1.5 (AM1.5) or AM0. Spectral response was performed using an Optronic Laboratories instrument, calibrated with a UV enhanced silicon detector. Refer to Appendix A for characterization calculations and performance measurements.

2.2 Poly (3-alkylthiophenes)

Poly(3-hexylthiophenes) composites with C60 PCBM are responsible for the recorded power efficiency.[14] Figure 10 shows the dramatic effect of the addition of PCBM to P3HT on the devices performances, which increases the open circuit voltage and current density.

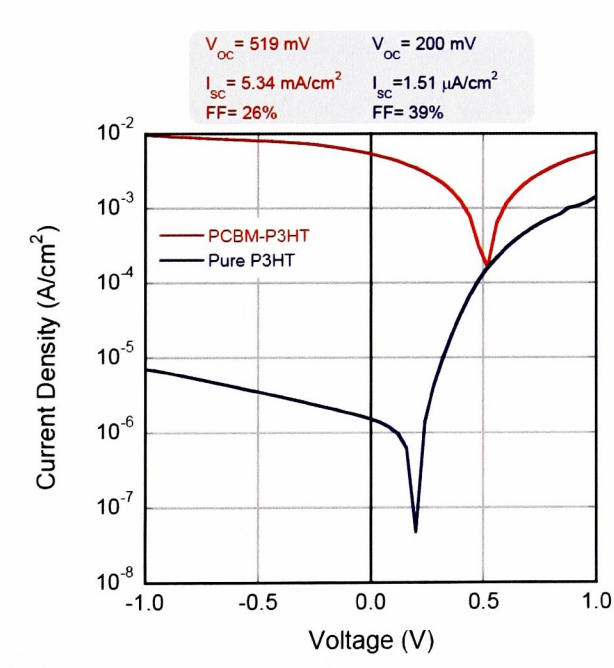

Figure 10: Effect of the addition of C60 PCBM on the current-voltage(I-V) curve for P3HT

Spectral response is useful to investigate the absorption limitation of the devices. From Figure 11, the photocurrent is only produced for P3HT:PCBM devices at energy higher than 2.0

eV which is consistent with the absorption of each component. This is not an ideal combination considering that the optimal energy is 1.4 eV.

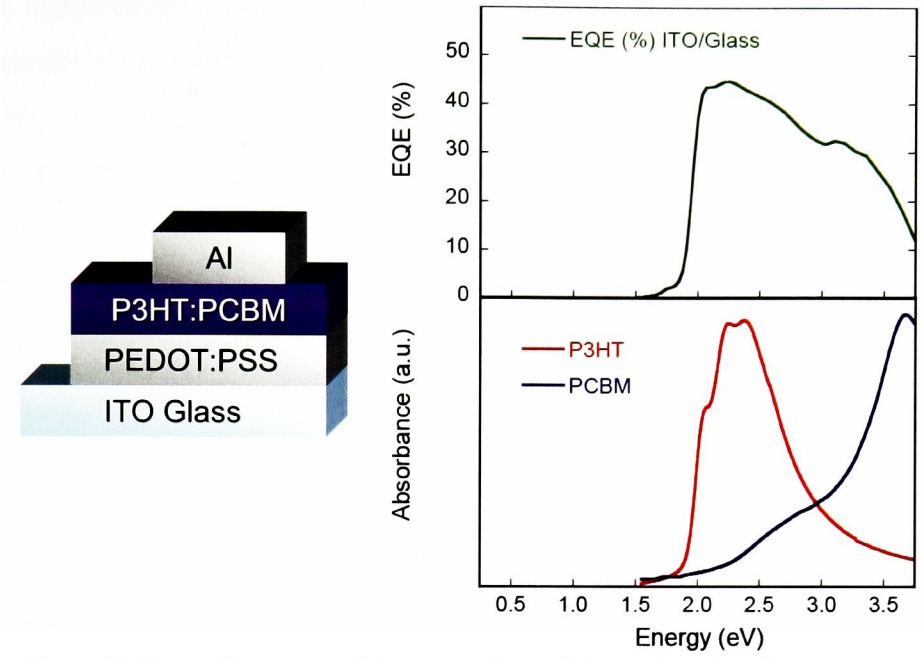

Figure 11: Spectral response of the composite and absorption of each component

One approach to obtaining an improved spectrum matching would include the use of a conjugated polymer with a larger absorption in the near-IR. The electrochemical bandgap for poly(3-alkythiophenes) (P3AT) is slightly larger with an increased side chain length[7] (Figure 12) and therefore other P3ATs such as Poly(3-buthylthiophenes) (P3BT) and Poly(3-octylthiophenes) (P3OT) have been compared to P3HT.

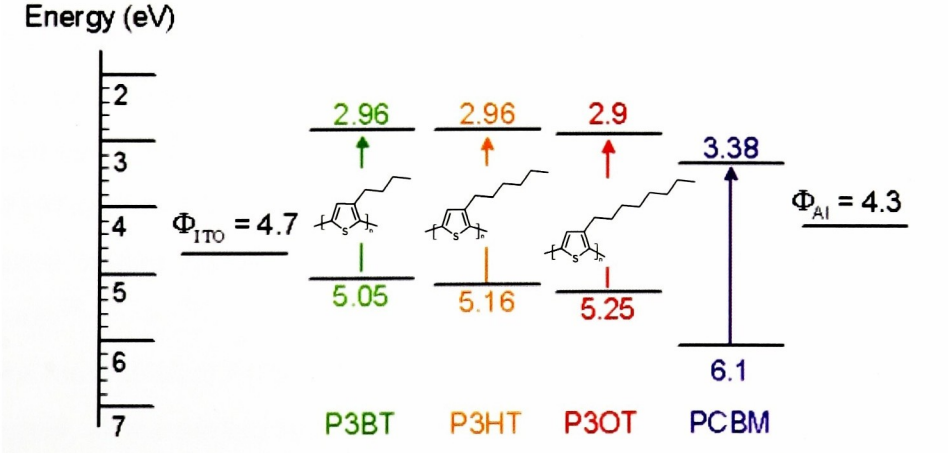

Figure 12: Energy levels for different poly(3-alkylthiophenes)[29,30]

2.3.1 Poly(3-alkythiophenes)/C60 PCBM composites

As hypothesized by the bandgap increase, the open circuit voltage of the P3OT devices compared to P3HT is higher. However, the current density of the P3OT devices is significantly less (Figure 13). Since all devices were made using the same annealing conditions (110°C for 1 hour), it is possible these conditions were not optimal for P3OT. Longer chains increase the bandgap, while lowering the absorption coefficient. Therefore, the increased chain length produces a change in the optimal thickness and microstructure needed to absorb most of the light[7] that should be optimized.

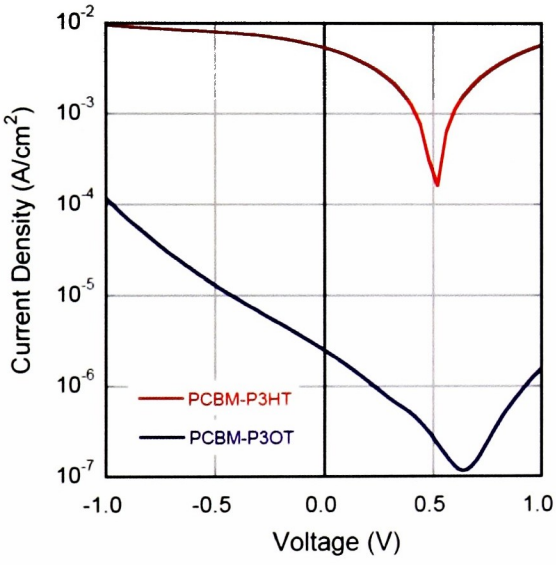

	J_{SC} (mA/cm²)	V_{OC} (mV)	FF (%)
P3OT	0.00243	637	14
P3HT	5.34	519	26

Figure 13: Comparison between P3HT: PCBM and P3OT:PCBM (1:1 ratio) Under AM0

As an alternative, poly(3-butylthiophenes) (P3BT) was considered in combination with P3OT. The bandgap of P3BT is lower than P3HT, therefore reducing the V_{oc}. However this reduced open circuit voltage may be increased by combining the P3BT with different ratios of P3OT such as 1:1, 1:3 or 3:1. The annealing time was lowered to 30 minutes based on published studies showing a faster degradation for P3BT than for P3HT at high temperature. [29]

The most efficient P3HT:PCBM device was obtained using the 30 minutes annealing time, however, all the devices had a lower efficiency than the devices made using P3HT. In addition, none of the devices exhibited higher open circuit voltage than P3HT. Devices

containing a larger portion of P3OT have a higher open circuit voltage than the 3:1 P3BT:P3OT which is consistent with the energy band alignment.

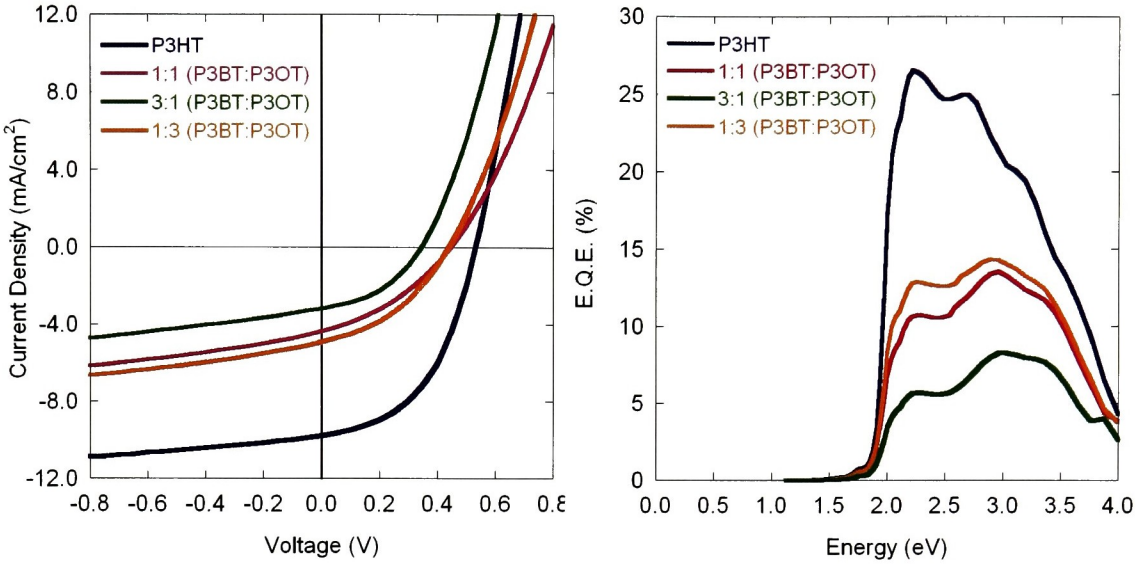

Figure 14: (a) Current Density measurements for different ratios of P3BT:P3OT by comparison to P3HT. (1:1 P3AT:PCBM ratio kept constant) under AM0 and (b) spectral response for the same ratios.

Devices made of a combination of P3BT and P3OT have better efficiencies than the pure P3OT devices (Figure 14). For the composite containing the higher percentage of P3OT (1:3 P3BT:P3OT), the current density was 5.9 mA/cm^2 compared to 2.43 μA/cm^2 for the P3OT alone. On the other hand, the open circuit voltage decreased from 0.637 V to 0.4 V due to the addition of P3BT.

2.3.2 Annealing and molecular weight

Among the numerous research teams working on organic solar cells, there does not appear to be an agreed standard for the optimal annealing conditions for P3HT:PCBM bulk heterojunctions. The lack of agreement is caused by the wide variance in the polymer regioregularity[13] and chain length[29] which affects its charge mobility and annealing conditions.

Low Mw P3HT has a limited photoresponse due to confinement of the conjugation length. For Mw around 10,000 g/mol, P3HT forms crystalline nanorods, which exhibit low charge mobility due to poor long-range interconnectivity of polymer chains. When P3HT Mw is higher than 30,000 g/mol, it forms nano fibrils which are connected over long distance (ca. 500 nm) which lead to an enhanced mobility.[29,31]

Due to its record efficiencies, P3HT has become the most studied polymer in solar cell studies. A recent study comparing the effect of molecular weight and performance of solar cells suggested the observed increased hole mobility in P3HT compared to P3BT may be due to different molecular weight and polydispersity of the P3BT samples. Both P3BT and P3HT have the same the π- π stacking distance between their crystallized chains, however P3BT packs more closely compared to P3HT across its interdigitated alkyl chains (1.26 nm and 1.64 nm respectively). Systematic study of the optimal annealing temperature for P3HT samples with various molecular weight and polydispersity has shown that the overall efficiency, as well as the optimal annealing temperature, increases with increasing molecular weight.[29] Therefore, the synthesis and characterization of other poly(3-alkylthiophenes) such as, P3OT and P3BT, is not as optimal as for P3HT. A lot of attention has been given to the regioregularity of the polymer, but only limited studies on the effect of the molecular weight. Actual molecular weight may be the most important factor in controlling annealing conditions and improving charge transfer.

The most typical effect of degradation in organic solar cells is the overgrowth of PCBM crystals.[3] Properties of P3AT diminish after over annealing due to a complete segregation of P3AT into unconnected nanorods for polymers of lower masses. The diminishing properties may also have been caused by electrode degradation due the higher temperature annealing required for high molecular weight materials. Polydisperse samples enhanced the ability of the polymers to self-organize on annealing at optimized temperatures.[29]

Studying the glass transition temperature of higher molecular weights P3OT and P3BT samples may give insight to the preparation conditions and optimal annealing temperature.

Due to the higher devices performances with the P3HT system, a side-by-side comparison of C60 and C70PCBM was conducted using this polymer. According to the energy level alignment, using the C70 instead of the C60 creates more allowed HUMO-LUMO transitions and therefore increases the current density.[32]

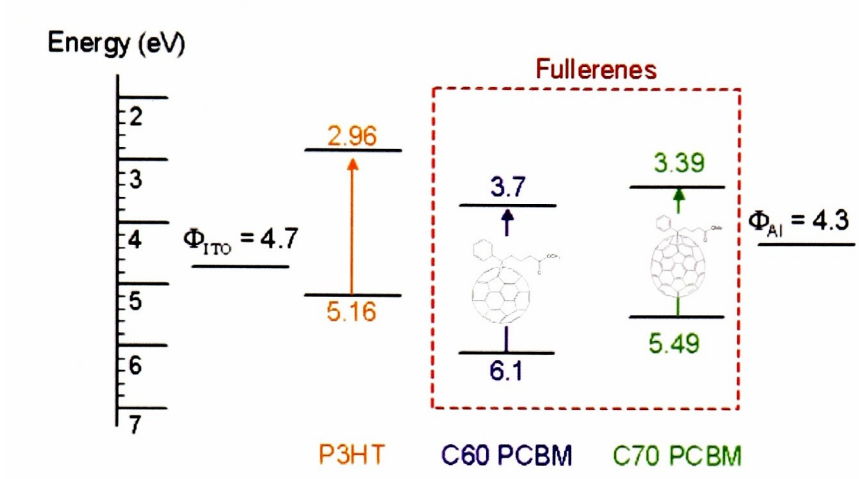

Figure 15: Energy level for C60 and 70 with P3HT

Using the C70PCBM resulted in increases in the current density and the open circuit voltage. This result is consistent with the different energy level of C70 and C60 (Figure 15). Annealing seems to have the same effect on both fullerenes since the fill factor is the same in both cases.

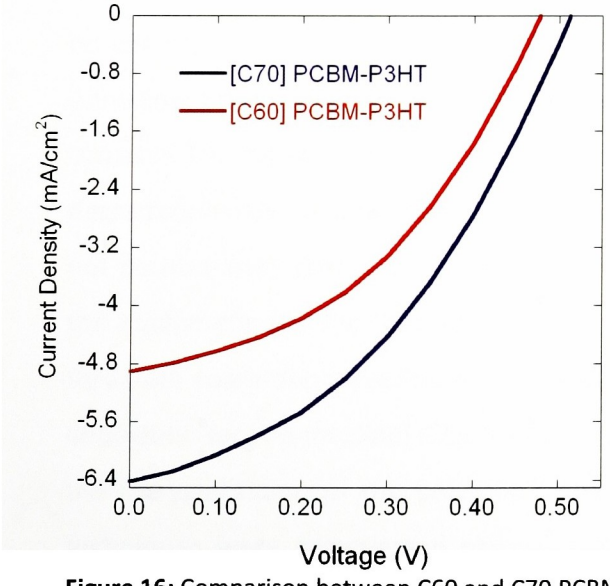

	J_{SC} (mA/cm²)	V_{OC} (mV)	FF (%)
C60	4.91	478	42
C70	6.41	511	41

Figure 16: Comparison between C60 and C70 PCBM with P3HT (1:1) Under AM0

The spectral response shows an enhanced quantum efficiency in the region between 1.6 and 1.8 eV as well as a broader shoulder in the high energy region (Figure 17).

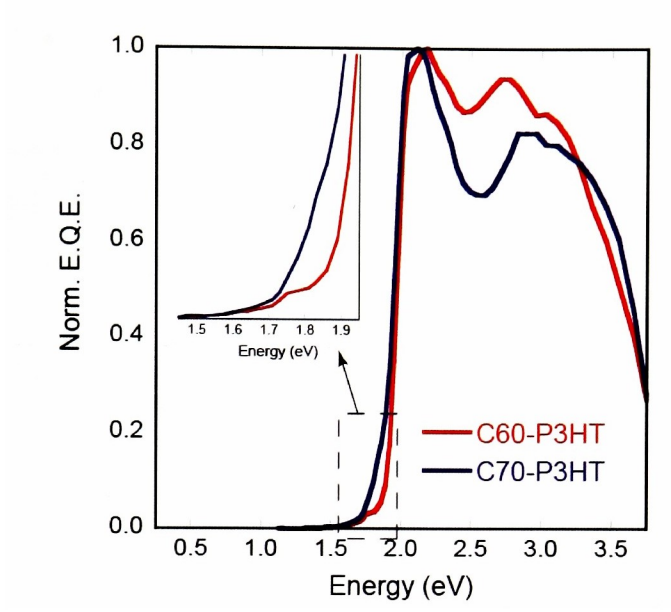

Figure 17: Spectral response of devices made using C60 PCBM and C70 PCBM with P3HT (1:1 w/w). In onset, the response from the C70 is enhanced for the lower energy

Published times for annealing conditions vary considerably between groups as a result of processing conditions and starting materials. Layer thickness of the active layer varies from 80 nm to 175 nm. Similar efficiency was obtained when temperature annealing ranges from 110°C to 158°C with time varying between 2 minutes and 2 hours.[3, 4, 33] There is no common agreement regarding what time interval the annealing should be performed. Annealing prior to the aluminum deposition (pre-annealing) creates an even surface for the contacts. On the other hand, since the organic layer is not protected yet by the aluminum, degradation may be faster than after the metal deposition. In some case, pre-annealing may not be necessary due to the equipment used for the contacts evaporation. Depending on the equipment and the throwing distance, some evaporators will generate more heat and therefore some pre-annealing may happen in the evaporator. Annealing after the contacts deposition (post-annealing) is generally performed at higher temperature since the goal is the recrystalization of the polymer.[33] Since these conditions vary between groups, both techniques were investigated using a 0.8: 1 PCBM/P3HT ratio based on the improved stability and high reproducibility attained by Ma et al.[3] For the regioregular P3HT purchased

from Rieke metals, and processing conditions described previously, the best-reward combination included pre-annealing at 110°C for 30 minutes under argon and post-annealing on a hot plate in a glovebox at 140°C for 30 minutes.

	Jsc (mA/cm²)	Voc (mV)	FF (%)	η (%)
No annealing	2.22	385	48.5	0.41
Pre-annealing	4.05	452	47.0	0.86
Pre + post annealing	5.06	570	51.4	1.48

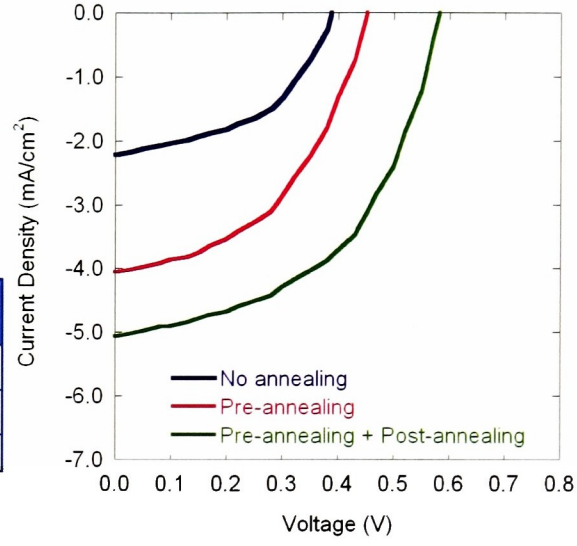

Figure 18: P3HT :PCBM (1 :0.8) in DCB with pre-annealing at 110 °C for 30 minutes under argon and post-annealing on a hot plate in the glovebox at 140 °C for 30 minutes. Tested under AM 1.5

Theoretically, the Voc should decrease with annealing. During annealing the π–π orbital interactions increase, resulting in heighted HOMO levels, and a reduced bandgap.[29]

In this study, the V_{oc} was increased during the first annealing as compared to the non annealed devices. Annealing at this lower temperature may have reduced the defects at the interface with the contacts and provided a superior metal deposition. Post-annealing was also necessary to achieve higher current density as well as a higher open circuit voltage.

The fill factor (FF) value indicates the internal resistance towards charges flow. The improved FF with pre and post annealing suggest a reduction in defects and the formation of fibrils during recrystalization, allowing the formation of pathway for charge transport.[31]

Since annealing causes phase segregation, a lower PCBM:P3HT ratio was chosen. In theory in order to obtain an enhanced crystallinity, annealing should be performed higher than the glass transition temperature of 110 °C for P3HT.[34] The improved crystallinity may have been observed using spectral response, since the features associated to PCBM

decrease while the features related to the polymer increases. With a lower ratio, the carrier transport became more efficient and carrier trapping is suppressed.[35]

In order to further improve the performance of poly(alkyl-thiophenes) devices, the effect of PCBM ratio in combination with annealing temperature should be investigated. Since crystallization has a dramatic impact on charge transport, techniques such as XRD, AFM and other characterization methods may be used to relate nanostructure ordering with annealing. Charge carrier mobility could also be studied using field effect transistors (FET), or other techniques to further investigate the effect of molecular weight and regioregularity. P3ATs with longer alkyl chains and higher molecular weight should be used in order to increase the open circuit voltage which currently limits the power efficiency.

2.3 MEH-PPV

Due to the high efficiency devices obtained using P3HT, little work has been done on MEH-PPV. Based on the knowledge developed with P3HT, the same concepts of molecular weight, solvent effects and thickness optimization were applied for MEH-PPV.

2.3.1 Chain orientation and thickness

The increased electrical properties of devices after annealing of the P3HT is due to the enhanced packing parallel to the substrate after recrystalization which is observed for regioregular samples.[13] Two factors strongly influence chains packing in MEH-PPV: the solvent and the molecular weight of the polymer. When the polymer is spin-coated from a solvent containing benzene rings, the chains will orient such as the side chains point inwards toward each other (Figure 19). Such orientation creates a highly ordered system. In non-cyclic solvents, the chains will have a twisted conformation which does not favor close packing of the chains.

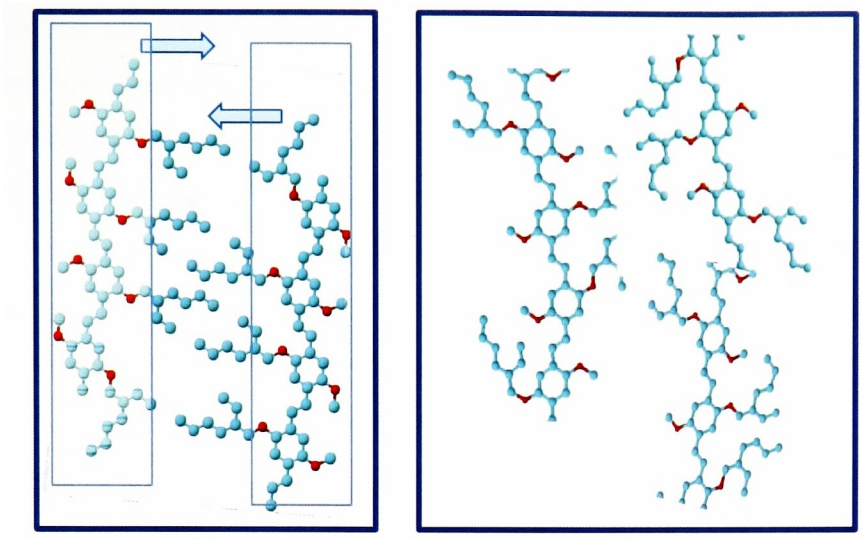

(a) (b)

Figure 19: MEH-PPV chain conformation when deposited from (a) a solvent containing a benzene ring and (b), without benzene ring

The improved nanostructure created by using a cyclic solvent has a direct impact on device performance as characterized by current-voltage measurements (Figure 20). *o*-xylene was chosen as the aromatic solvent since it has been shown that it results in better polymer chain stacking resulting in better electrical conduction.[36]

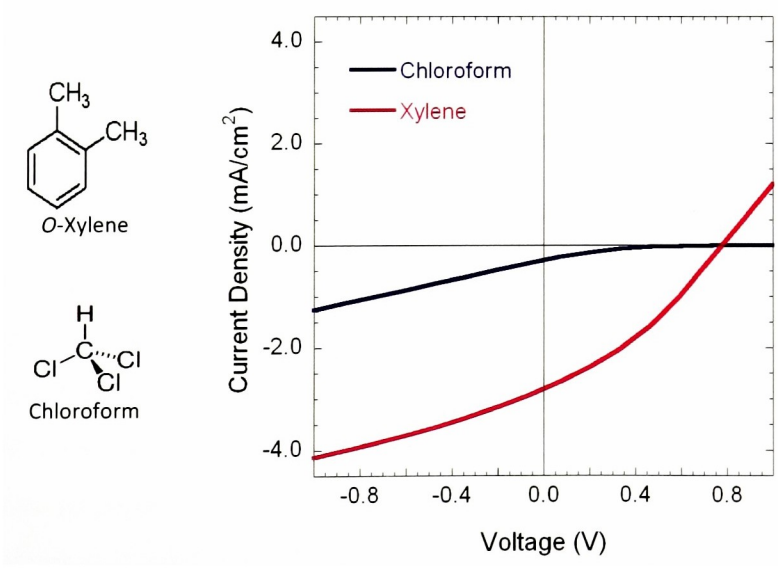

Figure 20: Current-density measurements of MEH-PPV:PCBM (1:4) spin-coated from a solution of *o*-xylene or chloroform

A second parameter influencing the orientation of the chains is the molecular weight. Most low molecular weight MEH-PPV have a random orientation of their chain segments, while the highest Mw have most of their chains parallel to the film plane. Similar to P3HT, the parallel orientation of chains may benefit charge transport. The refractive index and the absorption coefficients are also increased due to the parallel chain orientation.[37] Using the same conditions with a 4:1 PCBM:MEH-PPV weight ratio, the efficiency obtained with higher molecular weight is more than double the efficiency obtained from the lowest molecular weight combination.

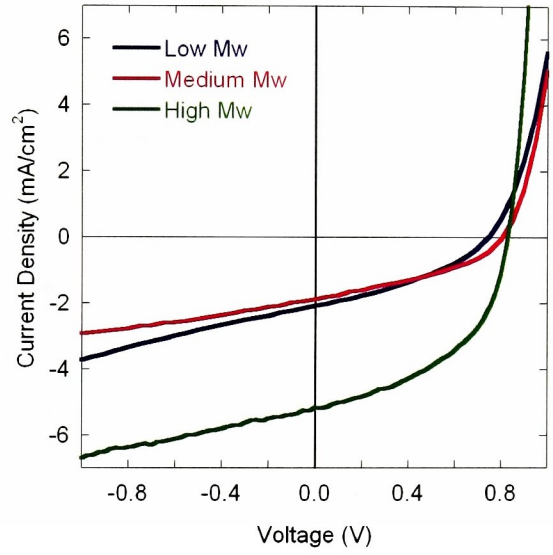

Mw	J_{SC} (mA/cm²)	V_{OC} (mV)	FF (%)	η (%)
Low Mw: 40,000 - 70,000	2.07	747	36.0	0.57
Medium Mw: 70,000 – 100,000	1.88	808	37.4	0.57
High Mw: 150,000 – 250,000	3.89	835	38.5	1.25

Figure 21: J-V Comparison of Mw effect on the performance of MEH-PPV:PCBM organic solar with a 4:1 weight ratio (Tested under AM1.5)

The same annealing was performed on all devices at low temperature. Annealing has been shown to deteriorate the devices' performances at temperature as low as 50 °C for 30 minutes. Since the glass transition temperature for MEH-PPV is 65 °C [38] by comparison to 110 °C for P3HT, lower temperature annealing should be used.

Since the absorption coefficient is affected by the molecular weight, the optimal thickness for effective charge transport was studied. Spin-coating speed has a direct effect on the performance of the devices due to the limited hole mobility in organic semiconductors. From the current-voltage characteristic graph, the open circuit voltage which is characteristic of the system, changes slightly with increasing deposition speeds.

However, the current densities as well as the FF increase substantially with higher speed, which corresponds to lower thickness. The maximum efficiency was obtained when the thickness was 130 nm as measured using a contact profilometer.

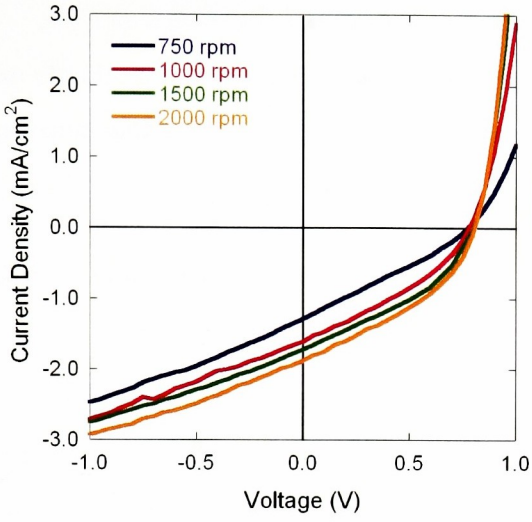

Speed (rpm)	Thickness (nm)	J_{SC} (mA/cm^2)	V_{OC} (mV)	FF (%)	η (%)
750	230	1.29	775	27.4	0.27
1500	200	1.72	802	32.6	0.45
2000	130	1.88	808	37.4	0.57

Figure 22: I-V curves of MEH:PPV-PCBM (1:4 by weight) spin-coated from *o*-xylene at different speeds.

The improved charge transfer in the polymer can also be observed using the spectral response data, where the peak associated with the polymer (around 2.4 eV) increases with a decrease in thickness.

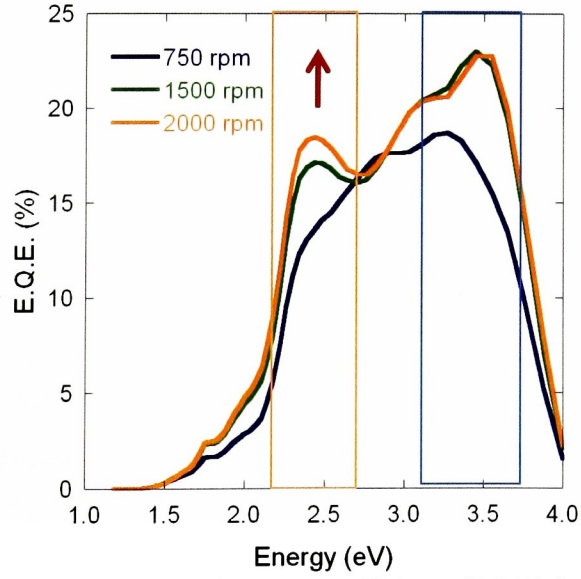

Figure 23: Effect of spin-speed on External Quantum Efficiency (E.Q.E.) for MEH-PPV:PCBM (1:4 by weight)

This enhanced response from the polymer illustrates the holes mobility limitation. For comparison, the features associated with C60PCBM (around 3.5 eV) increase from 750 rpm to 1500 rpm but stay constant when the speed is further increased.

The higher efficiencies are obtained with a thickness of 130 nm. Since annealing has an effect on the distribution of PCBM aggregates within the polymer, a thicker film could be possible with optimized PCBM ratio and annealing temperature.

2.3.2 Fullerenes optimization

Devices were fabricated using C70 PCBM instead of the C60 PCBM. This was done to test if the improved efficiency would be similar to what was previously observed with P3HT. In the case of MEH-PPV, the open-circuit voltage stayed constant, while the current density was considerably increased by the use of C70 PCBM instead of the C60. The efficiency from C60 to C70 rose from 1.25% to 2.06% which is substantially greater than the P3HT result.

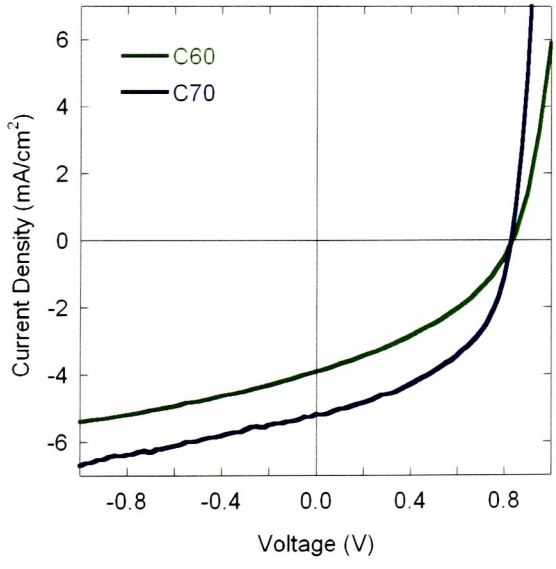

	J_{SC} (mA/cm²)	V_{OC} (mV)	FF (%)	η (%)
C60	3.89	835	38.5	1.25
C70	5.17	835	47.7	2.06

Figure 24: I-V curves for MEH-PPV with C60 PCBM or C70 PCBM (1:4 by weight). Tested under AM1.5

Based on the metal-insulator model, the addition of C70 should result in an increased open circuit voltage compared to the C60 based on their respective energy levels compared to the polymer. The interaction of conjugated polymers with fullerenes and the

energy of such systems should be investigated to understand the energy transfer process and the possible efficiency.

The effect of PCBM ratio was also considered in order to optimize the performance of MEH-PPV devices. The 1:4 weight ratio between MEH-PPV and PCBM is considered standard for most groups.[17, 39, 40] Based on the recent improved efficiency of P3HT devices due to lower PCBM content, the ratio was slightly lowered from 3 to 4 in order to find optimal conditions. From Figure 25, the current density is almost the same for a 3.5 or 4 ratio, while it is significantly lowered for a ratio of 3. The Voc steadily decreases when lowering the PCBM ratio. The optimal conditions are then the standard 1:4 ratio. Additional research would be required using various annealing conditions to optimize the PCBM ratio.

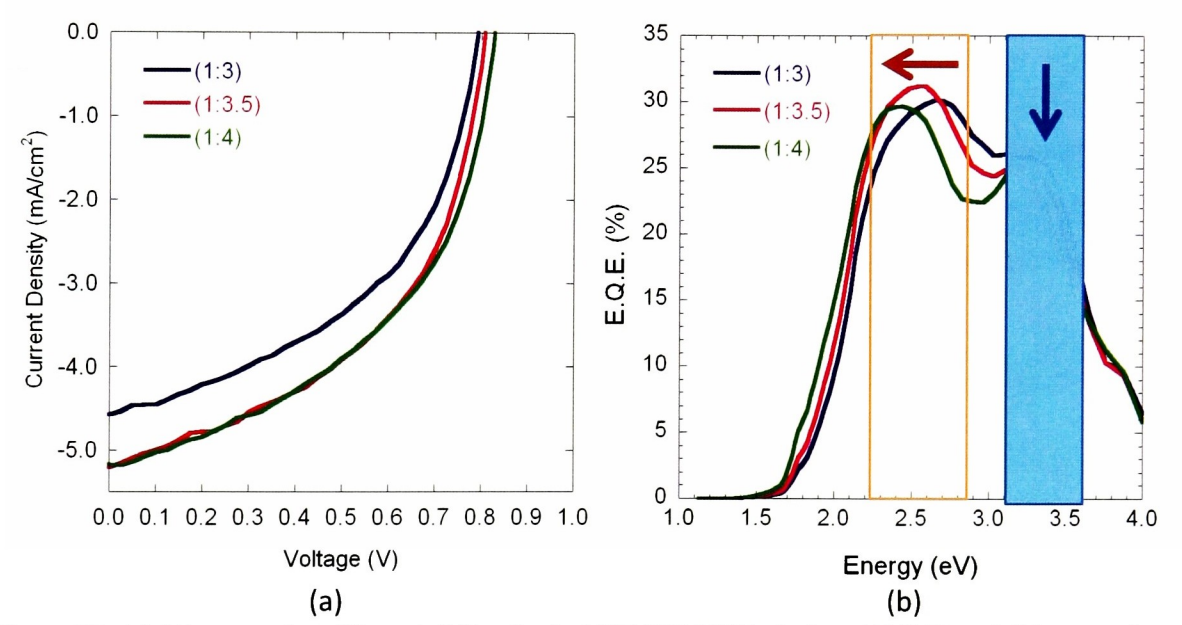

Figure 25: (a) I-V curves for different C70 ratio in MEH-PPV:PCBM devices (AM1.5) and (b) spectral response

From the spectral response, the PCBM peak (~ 3.4 eV) decreases with increasing PCBM ratio. The polymer peak (~2.5 eV) follows a different trend since it reaches a maximum for the 3.5 ratio. More interesting than the observed maximum of the polymer is the red-shift of this peak with increasing PCBM ratio. A shift toward the near-IR increases the theoretical efficiency of the devices due to the better matching between the solar spectrum and the polymer as shown in Figure 26.

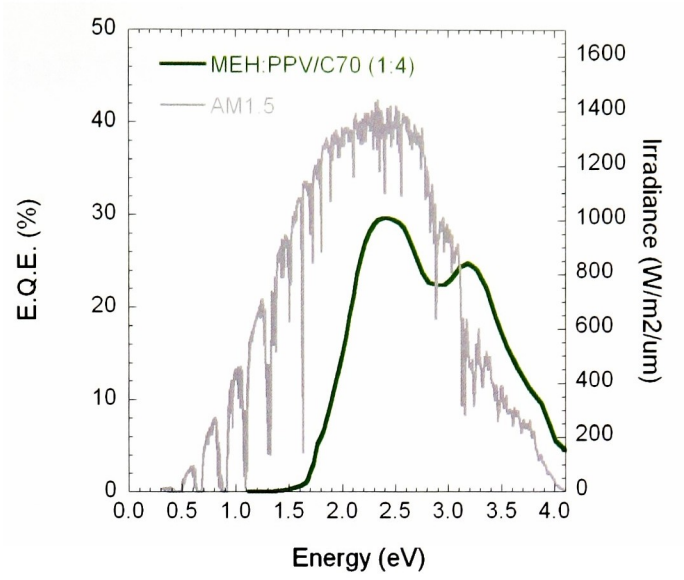

Figure 26: MEH-PPV/C70 optimal spectral response overlaid with the AM 1.5 spectrum

The effect of temperature on MEH-PPV has not been investigated to the same extent as on P3HT. Preliminary data on MEH-PPV indicated a decrease in performance and degradation after only 30 minutes at 80 °C. However with a higher molecular weight MEH-PPV, an annealing study could be beneficial and allow higher efficiency devices with higher fill factor.

Chapter 3: Quantum Dots

3.1 Experimental

3.1.1 Covalent synthesis of CdSe QDs

CdSe quantum dots are the most widely known and studied system due to their relatively simple synthesis and characterization. For this synthesis, 25.68 mg (0.2mmol) of cadmium oxide was added with 227.6 mg of stearic acid (0.08 mmol) and 2.54 mL of 1-octadecene (ODE) to a three neck flask connected to a Schlenk line following the established protocol.[41] The solution was pumped and purged 3 times before raising the temperature to 200 °C to obtain a clear solution. The flask was cooled to room temperature and 1.5 g (5.5 mmol) of octadecylamine (ODA) and 0.5 g of triocylphosphine oxide (TOPO) were added to the system and thoroughly degassed. The reaction mixture was raised to 280 °C where 2 mL of cold stock solution was injected (1 M TOPSe previously prepared in the glovebox). The reaction temperature was reduced to 250 °C and holded for one hour to obtain large QDs. The product was repeatedly washed in a separatory funnel using hexane and methanol until a bright top layer was obtained.

Since capping agents may suppress the charge transfer process, ligand exchange was performed on the QDs to replace the organic capping covering the nanoparticles with pyridine.[7, 22] Replacing the long chain fatty acid for a shorter element, such as pyridine, allows a superior contact between the donor and acceptor material. After precipitation and removal of the supernatant, a small amount of pyridine was added to the QDs, and the mixture was sonicated for 10 minutes prior to precipitation by hexanes. The ligand exchange was repeated 3 times before drying the QDs at 70 °C. The same ligand exchange process was used on all QDs systems prior to device fabrication.

Devices were fabricated using a 1:2 (MEH-PPV:CdSe) weight ratio in *o*-xylene. For all QDs, absorption spectra were performed on a Perkin Elmer Lamda 900 UV-VIS-NIR spectrometer. The PL spectra were performed on a Jobin Yvon Horiba Fluorolog

Fluorometer in order to obtain information about the electronic transitions (bandgap) and the size distribution of nanocrystals.

3.1.2 Non-covalent synthesis of InP nanocrystals

The colloidal synthesis was based on the non-covalent synthesis of III-V QDs developed by Peng.[25] InP QDs are currently the most sensitive system to the ligand length as well as to the presence of air and oxygen. In a typical reaction, 29.2 mg of indium acetate (0.1 mmol) was added to 68.5 mg of myristic acid (0.3 mmol) and 5 mL of ODE in a three-neck flask and heated to 120°C. The solution was pumped at this temperature for 1 hour to remove any moisture or air in the system. After repeated pumping and purging, the reaction flask was further heated to 300°C under argon. At this temperature, a 2 mL solution containing tris(trimethylsilyl)phosphine ($P(TMS)_3$) was injected (12 µL of $PTMS_3$ + 2 mL anhydrous ODE was prepared in the glovebox). The temperature was reduced to 270 °C for crystal growth and maintained for 30 minutes. The product was cleaned through a similar technique used for CdSe, while using a mixture of methanol and acetone (1:9) to precipitate and hexane to resuspend the QDs. Devices were prepared after ligand exchange using P3HT with a 1:1 weight ratio in DCB.

3.1.3 Covalent synthesis of InAs nanocrystals

InAs QDs were synthesized following established procedures using tris(trimethylsilyl)arsine with $InCl_3$. The synthesis of the tris(methylsilyl)arsine ($As(TMS)_3$) was adapted from literature.[42] In a typical synthesis, 1.7 g of sodium (73.5 mmol) was finely cut and added with 29.4 mmol of arsenic and 70 mL of anhydrous toluene into a 3-neck flask. The solution was heated to reflux while stirring for 48 hours. After cooling to room temperature, 73.5 mmol of chlorotrimethylsilane was added slowly to the reaction flask and then heated to reflux for an additional 24 hours while stirring.

After filtration, the resulting liquid was distilled to remove the excess toluene or any other volatile byproducts. Due to the high reactivity of the precursors, the QD synthesis was conducted in the glovebox. InAs QDs were prepared by injecting a $InCl_3$ solution mixed with $As(TMS)_3$ into Trioctylphosphine (TOP) at 300 °C, and the reaction flask was maintained at 260 °C for growth[43]. Aliquots were taken at regular intervals and quenched in anhydrous toluene for characterization (fluorescence and absorption). The product was cleaned using a toluene/methanol precipitation technique followed by resuspension. The In:As ratio was varied during the initial mixing before injection. The photovoltaic devices were made by dissolving the InAs QDs in a small amount of 1,2-dichlorobenzene (DCB) before being added in different mass ratios to the MEH-PPV and the PCBM. The reference MEH-PPV device was made using 7.5 mg/mL MEH-PPV in *o*-xylene. The weight ratios of MEH-PPV and PCBM were kept constant at 1:4 while different ratios of InAs QDs were added to the composite. An annealing step at 110 °C for 1 hour under argon followed the composite spin-coating.

3.2 CdSe Quantum dots

Due to their simple synthesis and focused size distribution, the first quantum dots investigated were CdSe. The principal difference between bulk crystals with an infinite size and quantum dots with a final size is the surface atoms, which possess dangling bonds that must be stabilized. In colloidal synthesis, the nucleation takes place immediately after injection and continues until the temperature and the monomer concentration drop below a critical threshold. The nucleation kinetics is difficult to study. After nucleation, there are two distinct kinetic regimes. First, during the focusing stage, the average nanocrystal size increases relatively rapidly and the size distribution is focused. When all the monomer in solution has been used for the QDs growth, the defocusing regime begins. The monomer concentration is lower than the nanocrystals concentration. Therefore, the smaller nanocrystals, which have the lower solubility, start shrinking and releasing monomer through Ostwald ripening. The bigger nanocrystals use the monomer in solution to continue their growth, which results in a broadened size distribution. To minimize this effect, coordinating solvents and ligands are used to protect the QDs and reduce the broadening.

The biggest QDs that could be prepared using this technique had an absorption around 2.1 eV. The repeated cleaning process has the advantage of removing most of the smaller QDs from the solution therefore contributing to a smaller size distribution and enhanced fluorescence. MEH-PPV was chosen as the conjugated polymer due to its lower absorption compared to P3HT which may allow the observation of sub-bandgap absorption around 2.1 eV. The energy levels of CdSe QDs and the polymer are well aligned, therefore, the devices' performances should be improved by the addition of the QDs.

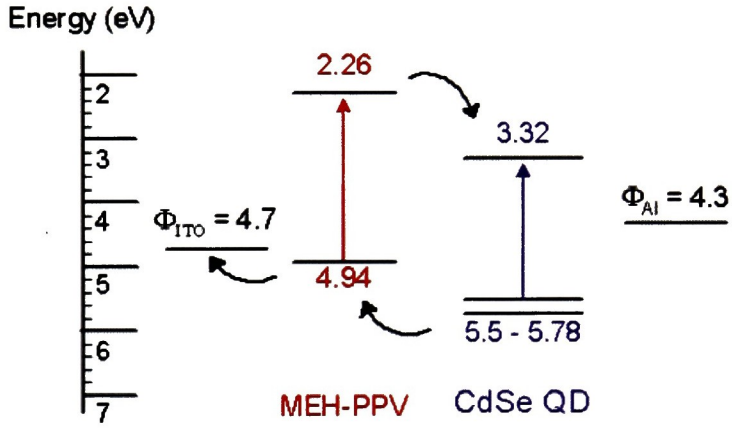

Figure 27: Energy level diagram for CdSe QD: MEH-PPV composites

The addition of CdSe QDs increases the current density when compared to the pure polymer. However, the performance of the reference device, a typical MEH-PPV:PCBM (1:4 weight ratio), is still superior in comparison to the composite containing the QDs. Currently only two groups have published results for CdSe: MEH-PPV composite blends. In one case, with a 90% wt of CdSe, the current density was approximately 2μA/cm^2 with a Voc of 0.72V,[24] while the other group used 80% wt of CdSe, and obtained current density of 2.6 μA/cm^2 with a V_{oc} of 0.58V.[23] In both cases, the performances of the devices are considerably lower than the devices prepared using our technique as shown in Figure 28.

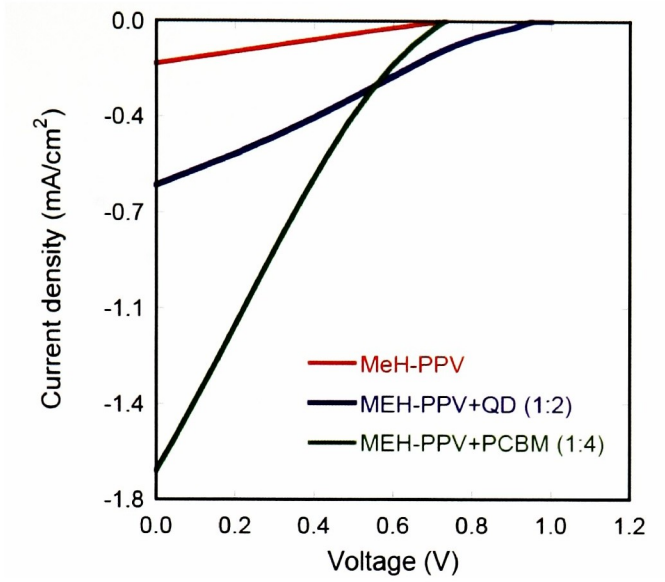

Figure 28: I-V curves for MEH-PPV with CdSe QDs and C60 PCBM in different ration. Tested under AM0

The addition of the CdSe QDs to the pure polymer increased both the current density and the open circuit-voltage. The current density difference between the different groups is most likely due to efficient charge transfer which is affected by ligand exchange. In theory, the Voc should be similar since the open circuit voltage should be a function of the energy level of the materials in the composite[3]. Using different sizes of quantum dots may slightly change the quantum dots bandgap, therefore changing the Voc but not sufficiently to explain a difference of 0.3 V between our measurements and those reported earlier. Surface defects or partial shunting of the devices may also lower the open circuit voltage. Considering that both the current density and the open circuit voltage were significantly higher than what was published by other groups, indicates better processing conditions that would therefore be applied for other quantum dots composites.

The QDs' size is close to the absorption edge of the polymer which results in the sub-bandgap absorption not able to be directly observed in the spectral response. However, the QDs improve the charge dissociation since the entire spectral response curve is increased and not only the region between 2 and 2.2 eV. In particular, the region between 3 and 3.8 eV is enhanced by the addition of the QDs compare to the pure polymer (Figure 29).

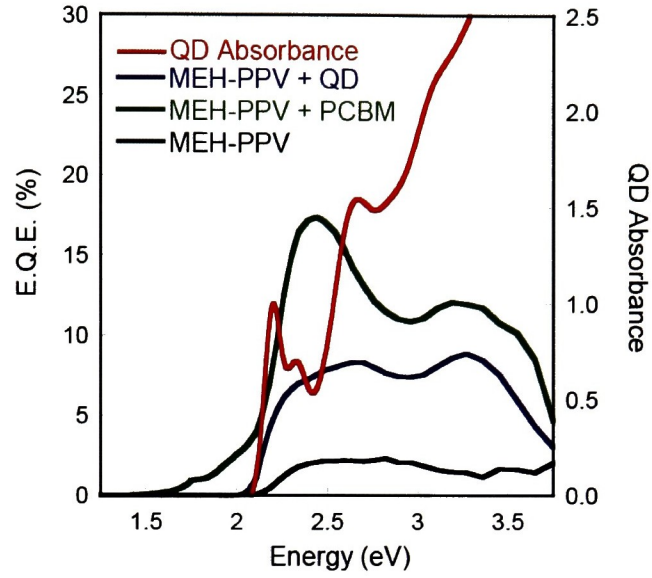

Figure 29: UV-vis spectra of the CdSe QDs used for the MEH-PPV:CdSe QDs composites with the External Quantum Efficiency (E.Q.E.) of the different composites.

Using QDs with lower energy absorption could result in sub-bandgap absorption. In order to do so, new injection of precursors at low temperature would be necessary to increase the monomer concentration and therefore allow further growth of the QDs. Since the growth temperature is considerably lower than the injection temperature, this technique can be applied for CdSe without formation of new nuclei.

These devices were primarily prepared to establish a fabrication procedure for composites devices made with QDs. This objective was successfully accomplished since the addition of CdSe QDs after ligand exchange demonstrated enhanced performance.

3.3 Indium Phosphide

Since indium phosphide QDs synthesis is simpler than other III-V systems such as InSb or GaSb, they were synthesized first in preparation for the InAs QDs using a non-coordinating solvent approach. For this technique, the reactivity of the monomers can be tuned by varying the ligand concentrations in the non-coordinating solvents. This tunable reactivity provides a way to balance nucleation and growth. This cannot be controlled by temperature alone since growth temperature needs to be close to the injection

temperature for III-V to provide high quality crystalline QDs. The optimal reaction involves a short and fast nucleation followed by a growth stage without new nucleation or ripening. Too long of a nucleation period will result in insufficient monomer left in solution to allow sufficient QDs growth and therefore result in unstable nanocrystals.[22] In the presence of excess ligands, these unstable nanocrystals will redisolve in solution.

The greatest results were obtained using the 3:1 ratio (indium acetate: ligand) and myristic acid as previously published by Battaglia et al.[25] As shown in figure 24, aliquots taken after 10 minutes do not show absorption compared to the aliquots taken after 30 minutes. However, after one hour, there is no clear indication of any shift in the absorption spectrum and the absorption peak appears to broaden. This is most likely caused by the lowering of monomers in solution creating Ostwald ripening.

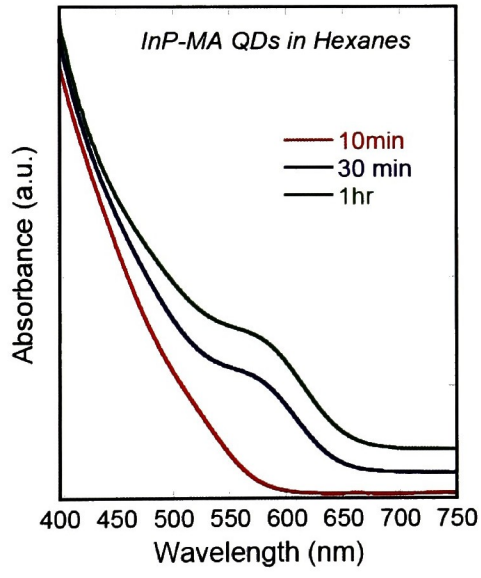

Figure 30: Temporal evolution spectra of InP QD

Bandgap engineering using InP QDs is limited . The bandgap stays almost constant with size by comparison to the CdSe that can be tuned through the visible spectrum. No significant improvement or growth was observed between a growth period of 30 minutes to 1 hour. Therefore, InP for device fabrication were prepared using a 30 minute growth. The absorption peak of these QDs shows an unambiguous absorption peak.

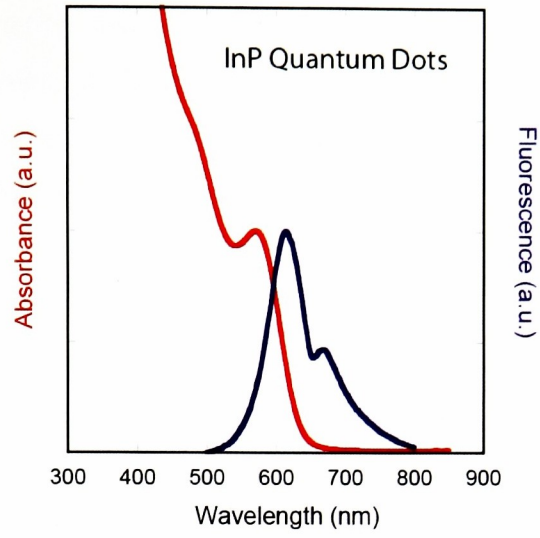

Figure 31: Fluorescence and absorption of InP QDs in hexanes after 30 minutes growth

The second absorption peak from the fluorescence spectra is associated with surface defects that can be etched using hydrofluoric acid process.[44] Etching was not performed due to the chemicals involved. The ligand exchange process was less successful for InP QDs than for CdSe. This was most likely caused by the chain length of the myristic acid protecting it. Devices were fabricated using a 1:1 ratio without ligand exchange and low current density (3.11 $\mu A/cm^2$) was obtained with P3HT polymer.

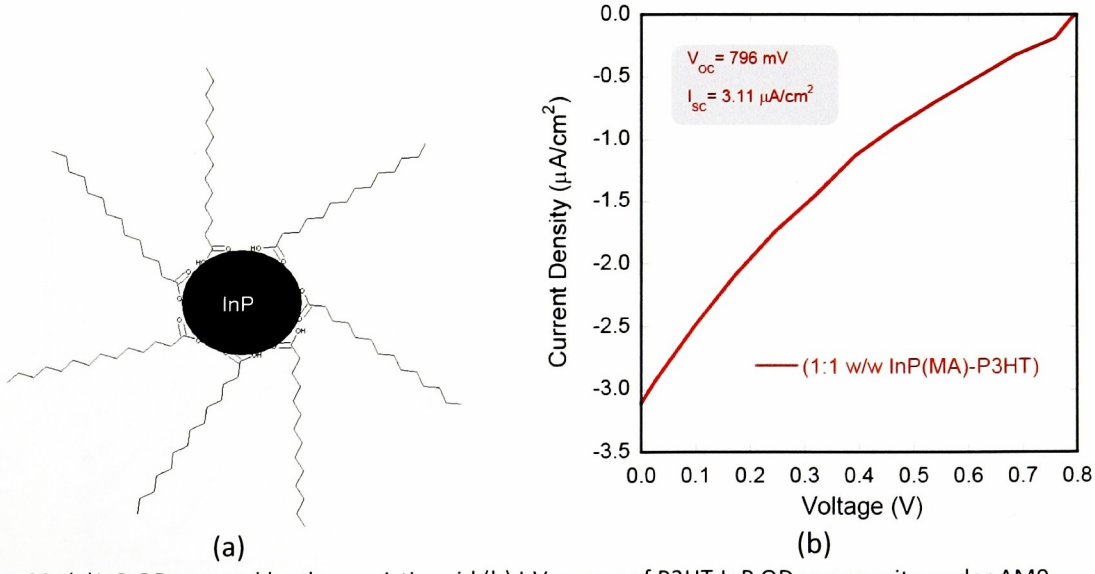

Figure 32: (a)InP QDs coated by the myristic acid (b) I-V curves of P3HT:InP QDs composite under AM0

Reduction in device performance by the addition of InP can be attributed to the ligand surrounding the QDs and interfering with charge transfer. The synthesis of InP

using the non-coordinating approach may be considered simpler than traditional organometallic approaches, however, the ligand exchange is a major issue for the fabrication of efficient solar cells device. Based on this issue, different approaches were considered for the synthesis of InAs QDs.

3.4 Indium Arsenide

The non-coordinating approach used for InP was applied for InAs without success. The coordinating approach using trioctylphosphine (TOP) was used since it was expected that the ligand exchange would be simplified in the absence of myristic acid capping the nanocrystals.

For the coordinating approach, nucleation must occur at high temperature followed by a lower temperature growth below a threshold point to obtain a narrow distribution of sizes. No ligands were used to protect the QDs during growth, resulting in observed broadening of the distribution in the as-synthesized QDs. Size-selective precipitation may be done to obtain a narrower distribution of QDs. This was performed on select samples to investigate the biggest possible QDs that could be produced.

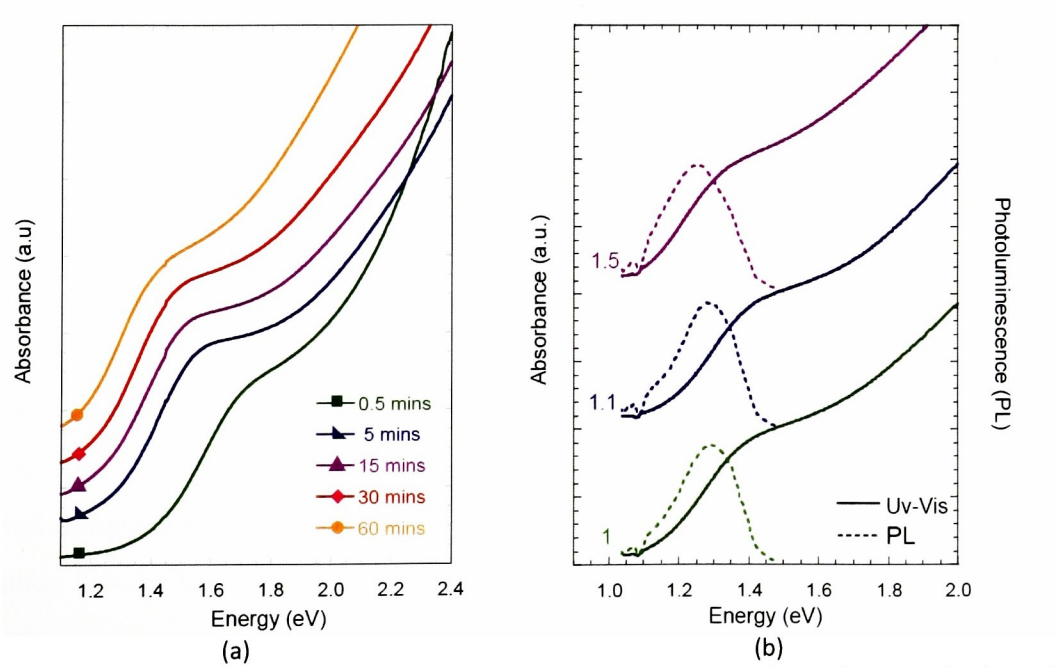

Figure 33: (a) UV-Vis spectra depicting temporal evolution of InAs QDs synthesized using a (1.1):1 ratio and (b) optical spectra of InAs QDs for different precursor ratios after 1 hour growth.

The InAs QDs show strong absorption when suspended in solution as colloids, however a requisite for polymer photodiodes is the concomitant absorption when dispersed in a polymer matrix. In order to understand this property, a series of InAs QD–MEH-PPV composites were prepared at different weight ratios and the optical absorption spectra were measured. The pyridine-capped InAs QDs were mixed with and subsequently ultrasonicated in MEH-PPV (solvent was *o*-xylene) before being drop-casted onto glass slides for analysis. Figure 34 shows the enhanced absorption in both the sub-gap region and high energy region due to QD absorption.

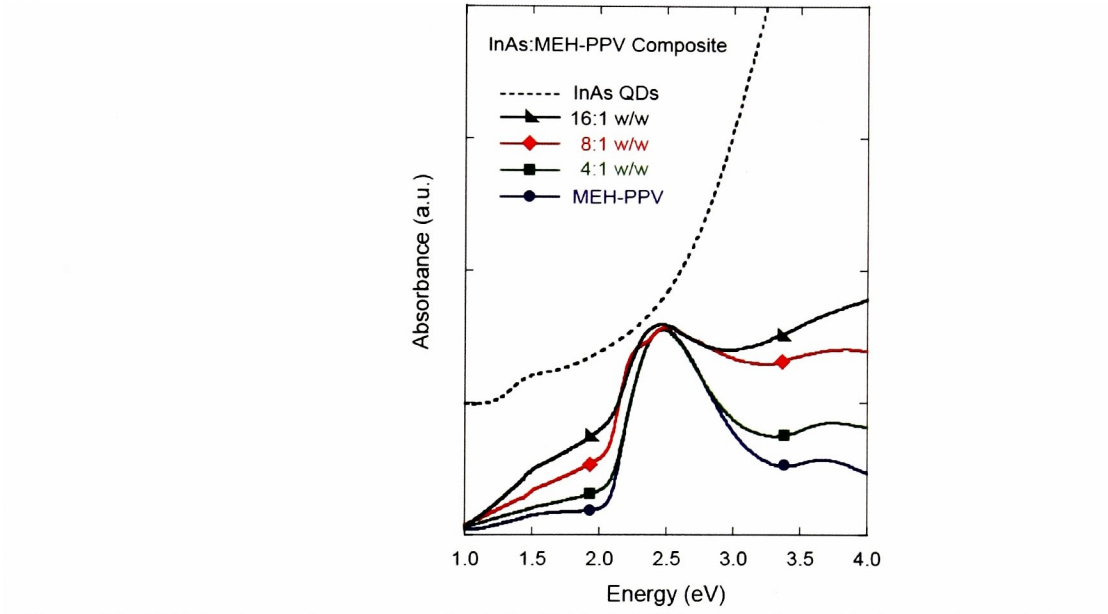

Figure 34: UV-Vis absorption spectra for InAs QD:MEH-PPV composites with increasing w/w loading of QDs. The dashed line represents the absorption spectrum for the starting QDs.

Although the highest absorption was observed with the 16:1 QD:MEH-PPV composite, the highest quality dispersions were observed in the 2:1 and 4:1 samples, respectively. Therefore, photodiodes were fabricated using these ratios in conjunction with PCBM to measure the AM1.5 conversion efficiency and spectral response. The InAs QDs prepared using a 1:1 In:As ratio were used for the fabrication of these devices due to their absorption around 1.3 eV where the MEH-PPV:PCBM composite does not exhibit spectral response.

The current-voltage results under simulated AM1.5 illumination are shown in Figure 35. The incorporation of InAs QDs produces a lower photoresponse compared to the control device, but, improves the fill factor substantially (>60%) with increasing concentration of QDs.

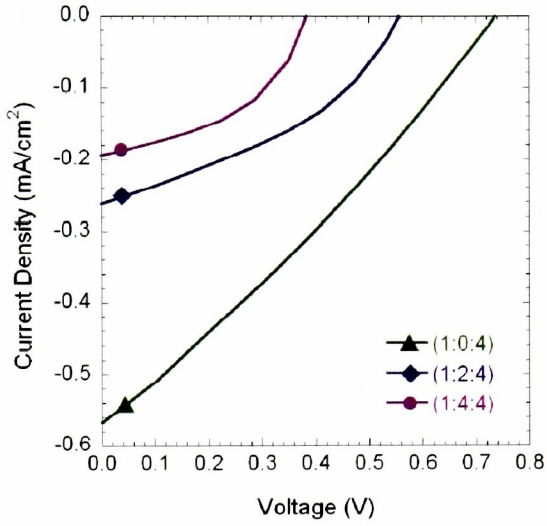

Figure 35: I-V characteristic for (MEH:PPV:InAs QDs:PCBM, by weight) under simulated AM1.5 illumination.

The spectral response data for these devices are provided in Figure 36. The devices with InAs QDs show a reduction in the EQE for both the MEH-PPV component centered at ~2.4 eV (refer to Figure 34 for MEH-PPV absorption) and the PCBM component at ~3.5 eV.

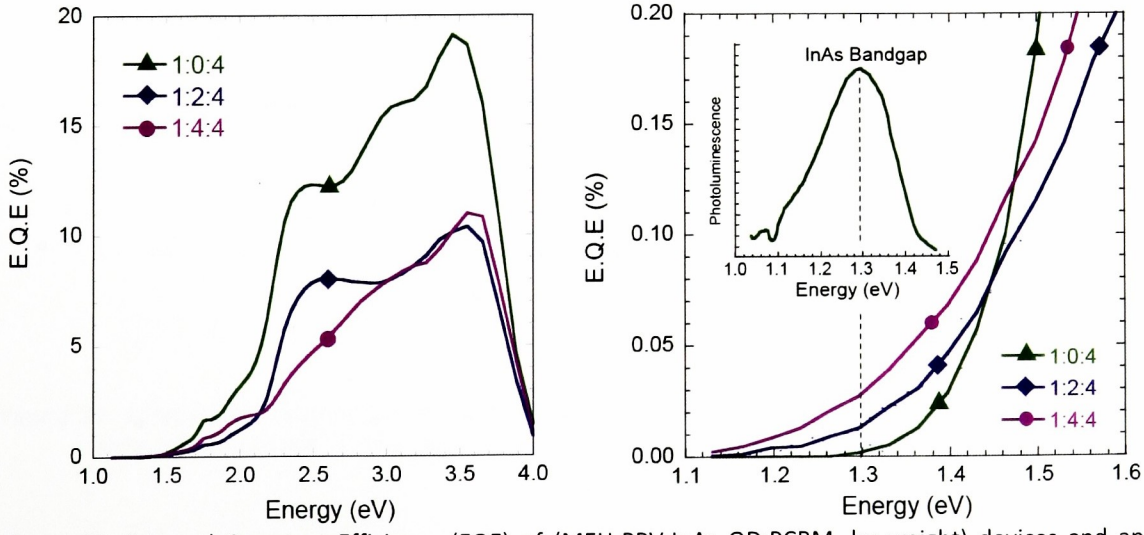

Figure 36: External Quantum Efficiency (EQE) of (MEH-PPV:InAs QD:PCBM, by weight) devices and an expanded region of the spectral response data below the polymer bandgap. The inset shows the typical PL spectra for InAs QDs with a bandgap of ~1.3 eV.

However, it should be noted that the InAs QDs quench the polymer absorption more significantly at higher concentration (1:4:4) compared to the PCBM, which is nearly equivalent for the two ratios used. Another result from this data set shown in Figure 36 is the apparent increase in photoresponse at ~1.3 eV, which correlates to the InAs QD bandgap.

Although the overall response is low, the sequential increase with addition of QDs supports the notion of using these materials for sub-polymer bandgap conversion, provided the overall efficiency can be improved. The reduction in photoresponse with the addition of InAs QDs has essential implications for optimizing these types of devices. Evaluation of the reported potential energy levels for the material components is shown in Figure 37, including the predominant carrier pathways. The two dashed lines represent the charge trapping that can occur by the InAs QDs when in concert with photo-induced MEH-PPV and PCBM, which leads to recombination.

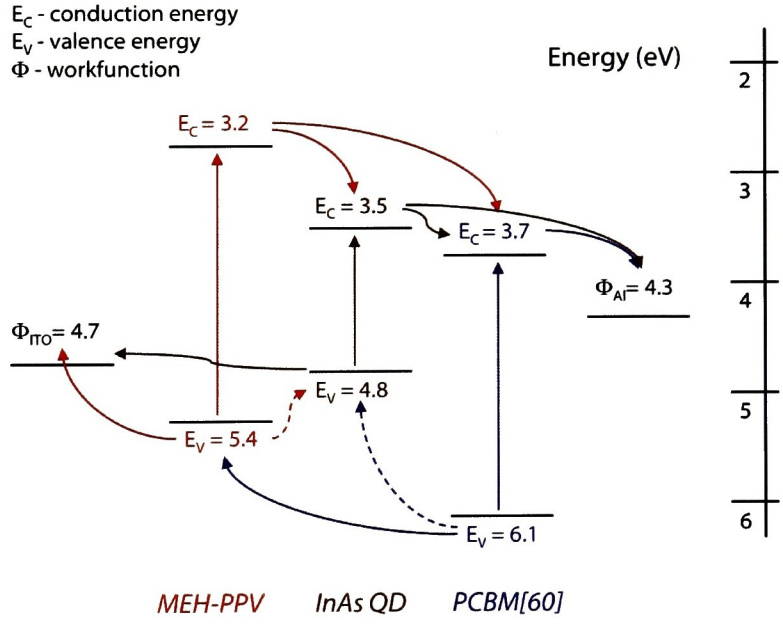

Figure 37: Energy level diagram for the composite devices (literature values extracted for InAs QDs[45] MEH-PPV and PCBM[46]). The dashed lines show device recombination pathways.

As is demonstrated in the diagram, this combination of materials is lacking the proper cascade of transitions for carrier transport (specifically hole). The photoresponse attributed to InAs QDs at 1.3 eV is energetically possible, and is expected to be low since hole conduction would presumably occur via hopping with neighboring QDs. Thus, the absorption below the polymer bandgap is a necessary first step (as seen in Figure 36), nevertheless, efficient charge transfer determines device feasibility. Utilization of InAs QDs for polymer solar cells has shown to be viable, but the selection of an appropriate conducting polymer and electrodes is ultimately required.

Chapter 4: Carbon Nanotubes

4.1 Experimental

Single-wall carbon nanotubes (SWNT) were fabricated by using the pulse laser vaporization technique and an Alexandrite laser.[30] SWNT were purified using a nitric acid reflux and thermal oxidation technique.[30] Multiwalls carbon nanotubes (MWNT) were fabricated using a chemical vapor deposition technique and used as produced.[47]

Based on previously published work by Landi et al. on SWNT and P3OT,[30] the maximum loading was chosen as 0.5% to limit shunting. The composite solution was made by first sonicating the carbon nanotubes in the solvent used for the chosen polymer (o-xylene for MEH-PPV and DCB for P3HT) until a uniform solution was obtained. The cut nanotubes were prepared using a piranha solution.[30]

Figure 38: Example of purified SWNTs before and after the cutting in a piranha solution

Finally, the HiPCO carbon nanotubes were purchased from Carbon Technologies Incorporated (CNI) and either used as received or were cut with the same technique used for the high purity SWNT.

4.1.1 *Intrinsic Layer Fabrication*

Two types of intrinsic layers have been investigated; PPV and pentacene. The PPV layer was obtained by spin-coating a cold solution of PolyphenyPoly(p-xylene tetrahydrothiophenium chloride) at 4000 rpm followed by a 2 hour curing at 180 °C.

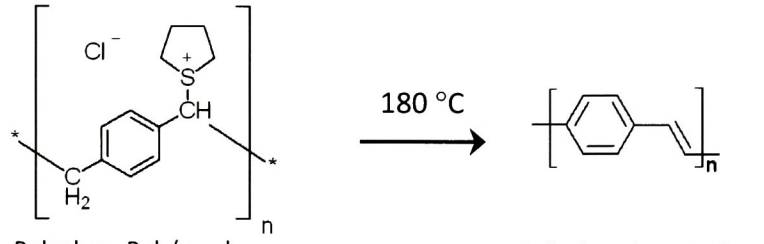

PolyphenyPoly(*p*-xylene tetrahydrothiophenium chloride)

Polyphenylenevinylene

Figure 39: PPV curing

Pentacene is a small molecule which is not soluble in most solvents. It was deposited through sublimation under vacuum at 120°C until a uniform layer was obtained using the setup shown in Figure 40.

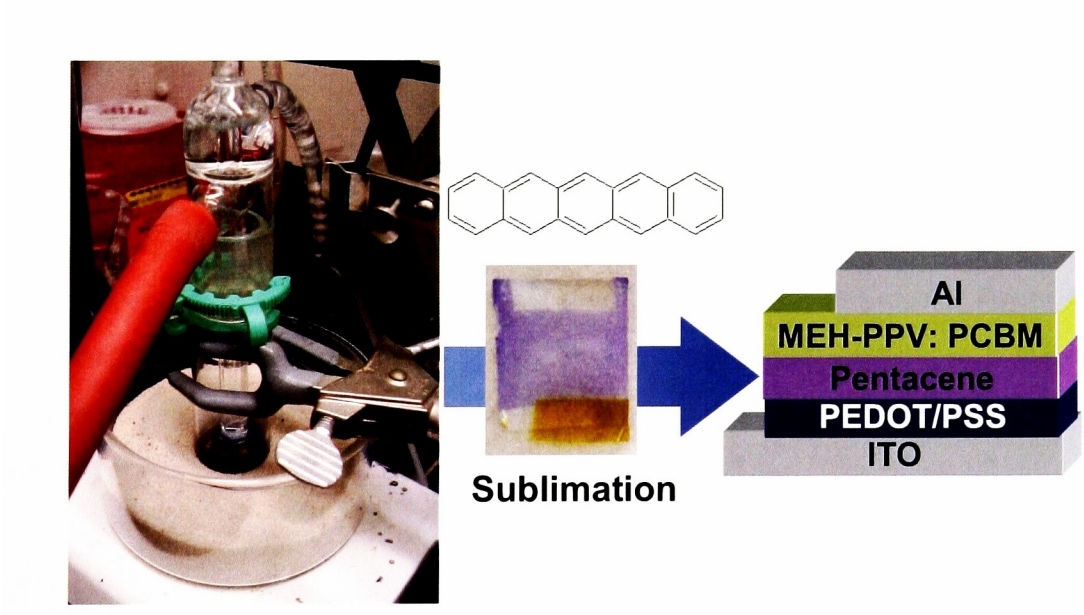

Figure 40: Sublimation process of pentacene on ITO and device structure fabricated using MEH-PPV:PCBM (1:4 by weight)

4.1.2 Aligned Arrays

Multi-walls carbon nanotubes (MWNT) aligned arrays were grown directly on ITO coated glass using chemical vapor deposition (CVD) under different conditions to obtain a transparent substrate coated with the MWNT.

Control Variables	Typical Conditions
Temperature	650 - 950 °C
Pressure	760 torr
Catalyst Composition	CP-Fe Dimer
Carrier Gas/Flow rate	0.5 – 2.5 L/min $Ar_{(g)}$
Catalyst Delivery rate	0.5 - 4.5 mL/hr
Catalyst Concentration	0.05 – 0.1 M
Injector Position	4 – 10 cm inside insert

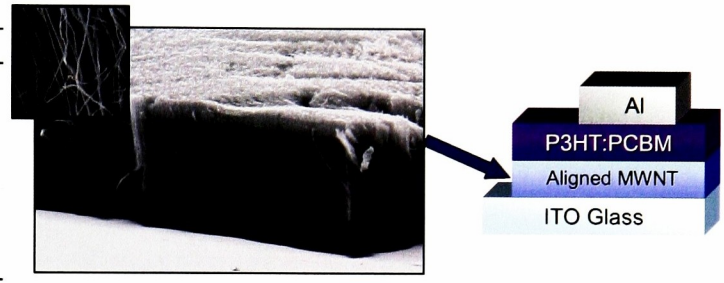

Figure 41: Condition for MWNT aligned arrays growth using CVD, Scanning electron micrograph of chemical vapor deposited multi wall carbon nanotube array on indium tin oxide coated glass and photovoltaic structure.

The active layer was then spin-coated on top of the array with and without an additional PEDOT: PSS layer. The composite chosen was P3HT:PCBM with a 1:1 ratio since thicker devices may be produced with this polymer in comparison to MEH-PPV.

4.2 Laser produced carbon nanotubes composites

Devices were fabricated using P3HT with the addition of C60 PCBM to investigate charge dissociation and transport in organic solar cells. However, as shown in Figure 42, for a series of devices fabricated with a P3HT to PCBM ratio kept constant at 1, the device performance decreased significantly with increasing SWNT content. Devices with SWNT content above 0.5% were completely shunted.

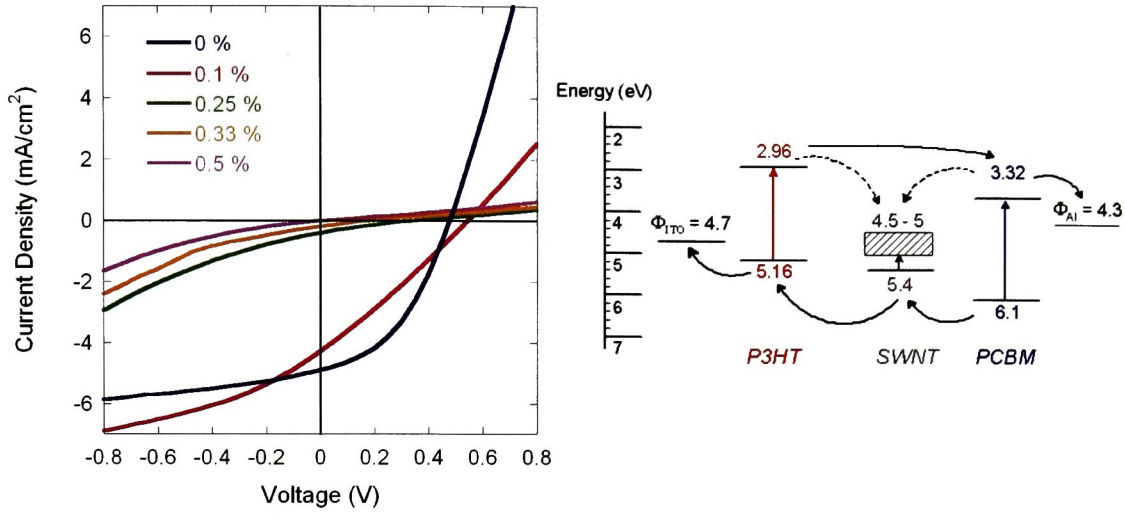

(a) (b)

Figure 42: (a) % SWNT in 1:1:PCBM under simulated AM0 and (b) energy diagram of the composite with possible recombination pathways

SWNT length may cause electron percolation between the Al contact and the PEDOT-PSS layer or the ITO layer. There is also the possibility of the SWNT acting as recombination pathways throughout the active region of the device.

Shunting might be due to the contact of the Al contact with the ITO. Therefore, two different types of carbon nanotubes with different length were compared to the laser-produced laser carbon nanotubes. As shown in Figure 43, the cut HiPCO carbon nanotubes give better results than the regular HiPCO carbon nanotubes.

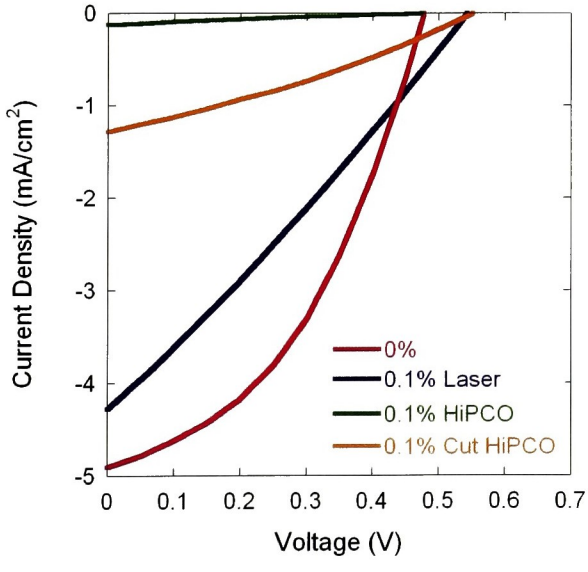

Figure 43: I-V curves showing the effect of cut SWNT

Therefore the length reduction of the carbon nanotubes may be an interesting technique to incorporate these nanomaterials into photovoltaic devices.

For the purified SWNT, the low open circuit voltage might not only be due to shunting due to carbon nanotubes touching the electrodes but also due to the polymer type. Therefore MEH-PPV was compared to P3HT with HiPCO. For the same carbon nanotubes loading, the V_{oc} of the devices made from MEH-PPV is considerably higher than for P3HT, while the current density is the same. The current density may also be increased by the addition of a higher concentration of carbon nanotubes with only a small decrease in V_{oc}.

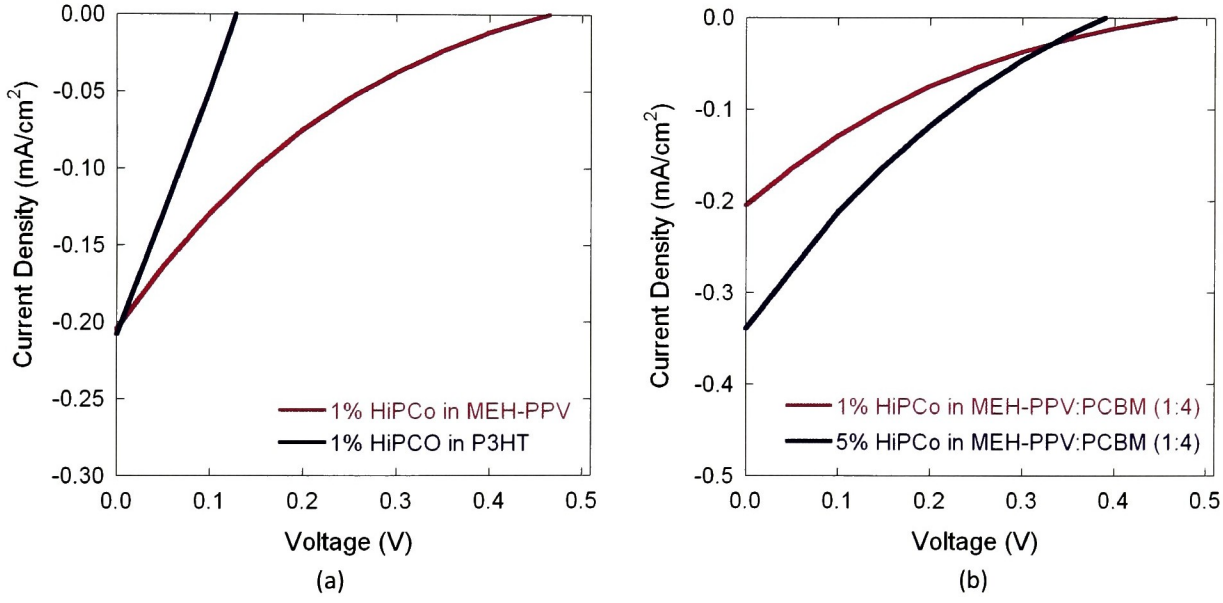

Figure 44: (a) Polymer Comparison MEH-PPV:PCBM (1:4) - P3HT: PCBM (1:1) and (b) effect of the increasing of SWNT in MEH-PPV devices for MEH-PPV: PCBM (1:4 by weight)

The V_{oc} is related to the difference between the LUMO of the acceptor and the HOMO level of the donor. The HOMO of MEH-PPV is 5.4 eV compared to 5.16 eV which may explain the increased open circuit voltage from the composite using MEH-PPV instead of P3HT. The combination of both PCBM and SWNT may cause trapping of the charges instead of charge dissociation due to the energy level of the LUMO of the SWNT compared to the lower energy LUMO level of the PCBM.

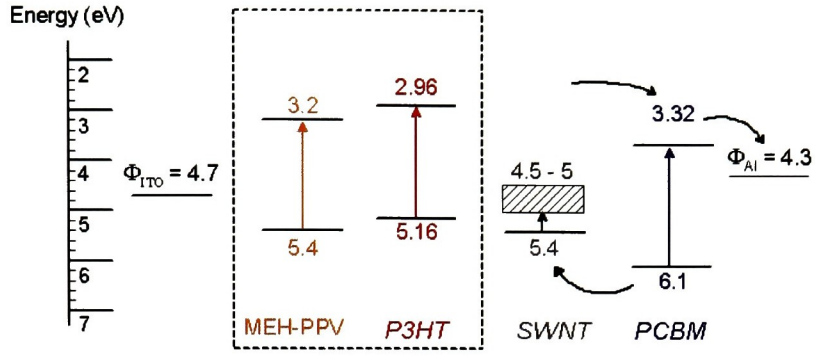

Figure 45: Energy diagram for different conjugated polymers with SWNT and PCBM

Finally, MWNT were introduced into the bulk heterojunction to enhance charge transport. The bulk heterojunction was made using MEH-PPV based on the higher doping previously obtained. Figure 46 shows higher devices performances when using MWNT rather than SWNT. From the spectral response (Figure 46b), the addition of MWNT appears to improve holes collection since the features associated with the polymer (~2.4 eV) are increased by comparison to the 1% MWNT, while the regions associated with PCBM (~3.4 eV) stay almost constant.

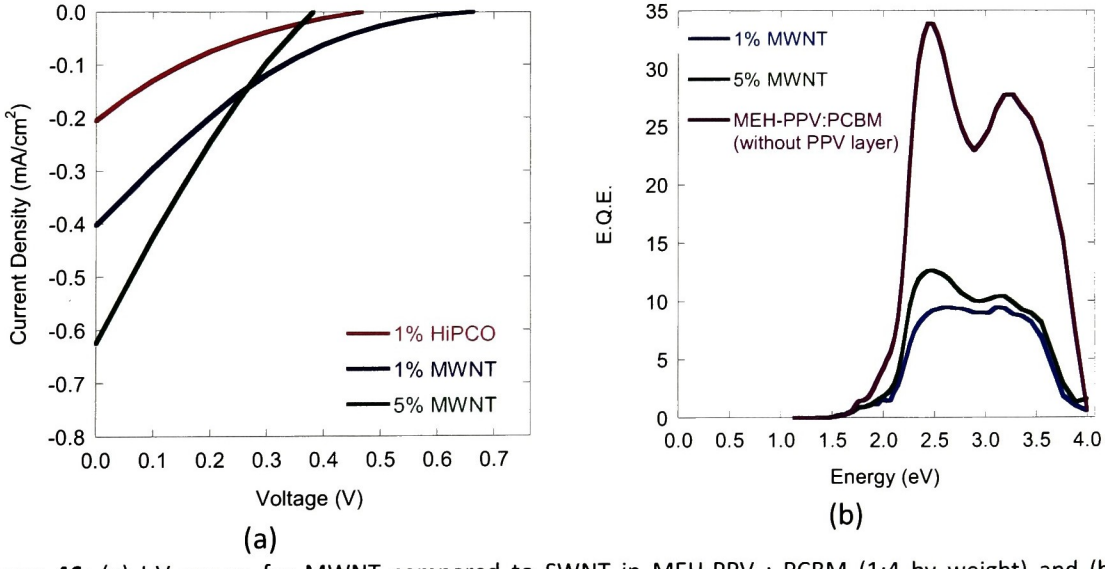

Figure 46: (a) I-V curves for MWNT compared to SWNT in MEH-PPV : PCBM (1:4 by weight) and (b) spectral response

Therefore, MWNT may be a more viable option in organic solar cells in combination with PCBM and conjugated polymers as compared to SWNT. By improving the optimal

composition and length of the tubes, MWNT could be used to improve the holes collection, especially in polymers with low holes mobility such as MEH-PPV.

4.3 Intrinsic layer

The deposition of an intrinsic layer before the deposition of the active layer was investigated as an alternative approach to prevent device shunting. The active layer is spin-coated from DCB, therefore the intrinsic layer should not be soluble in polar solvents. For this reason, Polyphenylenevinylene (PPV) was chosen since it can be converted from solution to a non-soluble compound.

As shown in Figure 47, the PPV layer allows a higher SWNT loading with higher current density, however the open circuit voltage is lowered considerably by the addition of the SWNT. The current density remains lowered as compared to the original devices.

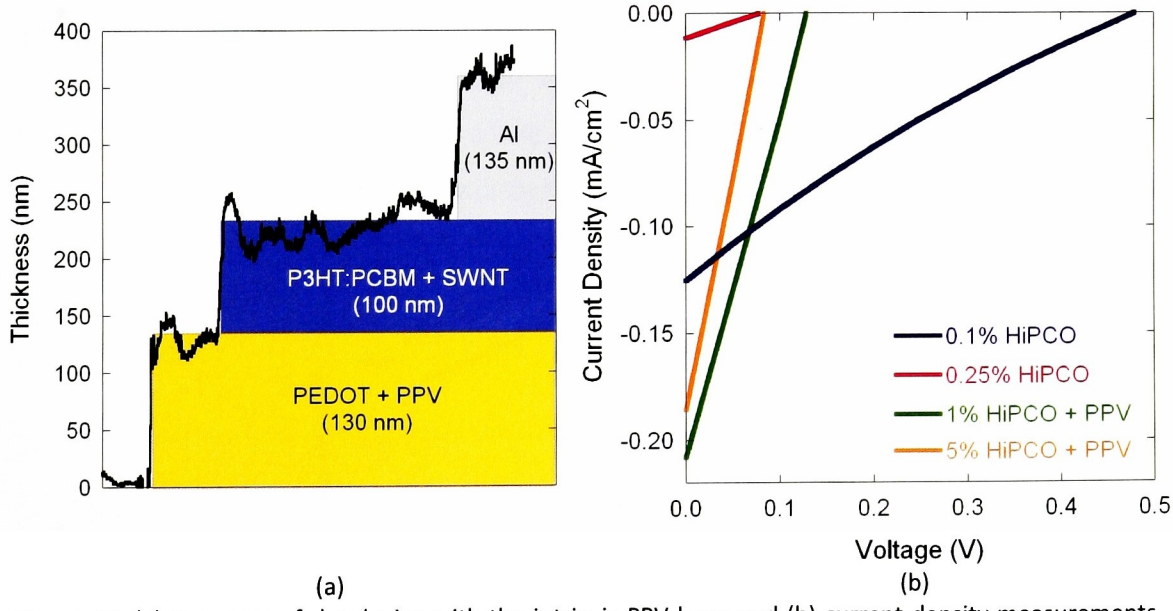

Figure 47: (a) Structure of the device with the intrinsic PPV layer and (b) current-density measurements with HiPCO SWNT.

As shown in Figure 38, the energy level of the PPV is not properly aligned with the other elements in the system and recombination may therefore explain the low V_{oc}.

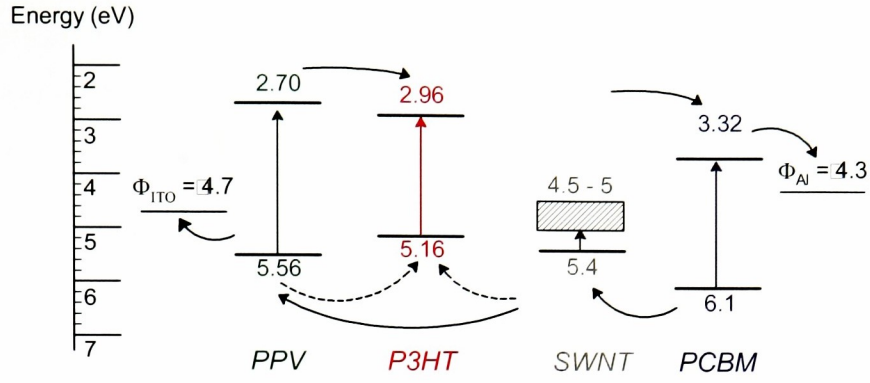

Figure 48: Energy level diagram for PPV/P3HT:PCBM:SWNT devices (literature values for SWNT[30]).

A second intrinsic layer made of Pentacene was also studied. Pentacene is insoluble in most organic solvents at room temperature. Therefore it must be deposited through sublimation under vacuum. The actual layer thickness was difficult to control due to the inability to observe the sample during deposition based on the experimental setup. Samples with similar covering were used for device fabrication. Due to the sublimation technique used, the surface was mostly composed of powder and therefore was partly removed during the deposition of the active layer. MEH-PPV was chosen as the polymer to minimize this effect since DCB removed the entire pentacene layer. The addition of the pentacene layer did not improve the performance significantly.

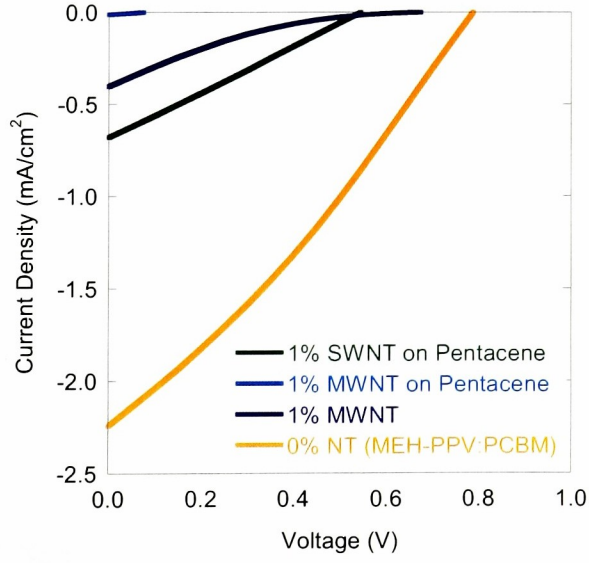

Figure 49: I-V for 1% carbon nanotubes (SWNT or MWNT) with and without the Pentacene layer in MEH-PPV: C60 PCBM (1:4 by weight)

The addition of a pentacene layer through a different technique should be examined since the energy transfer is favorable with this intrinsic layer as shown in Figure 50 for P3HT. Since the principal limitation is the deposition technique, using a soluble derivative that can be converted using heat treatment should be considered.[48]

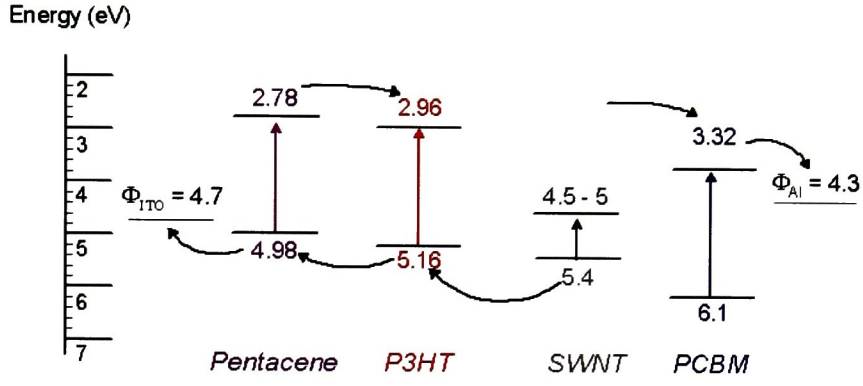

Figure 50: Energy diagram of pentacene intrinsic layer with P3HT/SWNT/PCBM composite (literature value for pentacene.[49]

4.4 Aligned Arrays

Aligned multi wall carbon nanotube arrays were used to produce solar cells using the same P3HT: PCBM (1:1) active layer. In order to correctly serve their role of conducting electrodes, the MWNT aligned arrays should be short enough to penetrate the polymer layer without touching the top electrode. At the same time, shorter arrays keep the optical transmission maximal which is essential for photon absorption. Figure 44 illustrates this requirement. On the left, short MWNT keep the substrate transparent and allow uniform deposition of the polymer. On the right, long MWNT reduce light transmission considerably. Devices made from arrays produced under these conditions were all shunted. The Normarski micrograph shows the topography of the layer and in particular, in green, the carbon nanotubes which are not covered by the polymer.

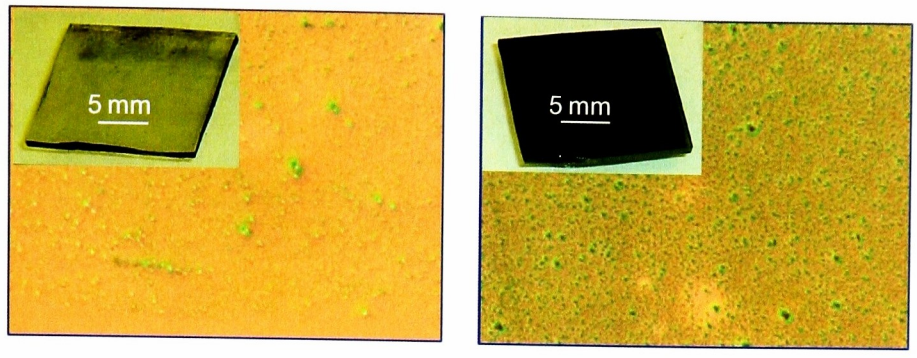

Figure 51: Nomarski micrograph (10X) of MWNT aligned arrays covered with P3HT:PCBM (1:1) active layer. The green color represent MWNT going through the polymer.

To prevent the MWNT contacting with the Al, some devices were spin-coated first with PEDOT on top of the array. Since the PEDOT:PSS solvent is water, there appears to be no dissolution of the underneath array. The addition of PEDOT:PSS had no impact on the current density but increased the V_{oc}.

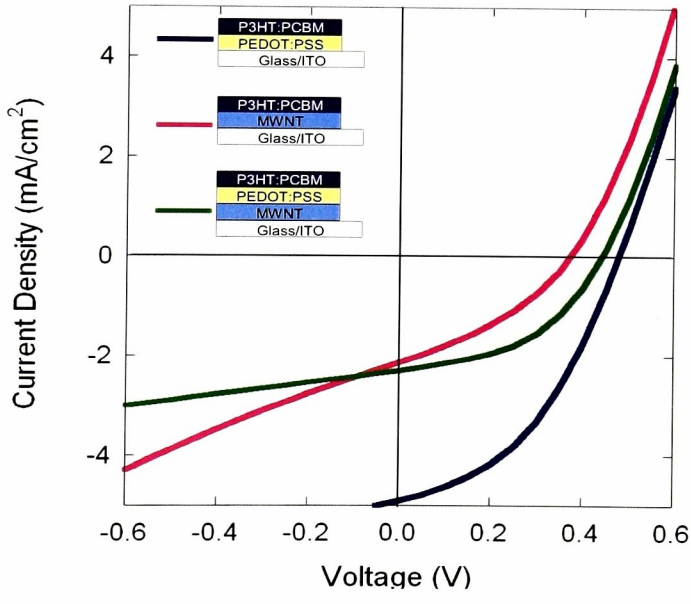

Figure 52: Schematic device diagram and current-voltage measurements (AM 1.5)

The lowering of the current density compared to the control device can be explained by the reduced light absorption. The reduction in open circuit voltage is consistent with what was observed from other groups and is attributed to the difference in work function from the MWNT and the ITO.[28]

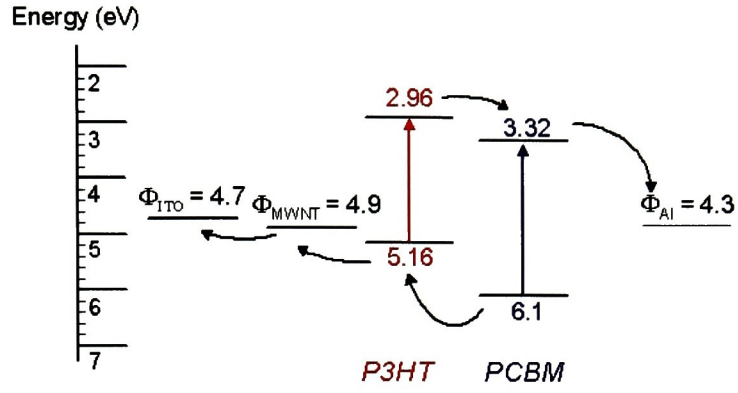

Figure 53: Energy level in MWNT aligned array with P3HT:PCBM composite

An encouraging point is the shape of the I-V curve which does not indicate shunting. Therefore, with increased control on the length and by increasing the uniformity of the arrays on ITO, MWNT aligned arrays could be used as hole-extracting electrodes. However, since the work function of MWNT is higher than the ITO, another system such as MEH-PPV C60 or MEH-PPV C70 may yield higher efficiencies.

Conclusion

Organic solar cells performances are mainly limited by the photon absorption due to the mismatch between the conducting polymer and the solar spectrum as well as the exciton diffusion since generated excitons are not efficiently dissociated into free charges. Nanomaterials such as fullerenes, quantum dots and carbon nanotubes were investigated in combination with conjugated polymers to allow for a broader harvesting of the solar spectrum. Since exciton diffusion is directly related to the nanomorphology of the composites, the processing conditions were studied, in particular for the MEH-PPV:PCBM composite.

Composites of fullerenes and P3HT are responsible for the record efficiencies. Factors, such as high molecular weight and regioregularity, have a dramatic effect on chain orientation and the ordering of polymers chains through annealing process. Other poly(3-alkylthiophenes) do not perform as well as P3HT and this difference may be attributed to the limited study of the optimum conditions for charge transfer in those polymers. For both P3BT and P3OT, only low Mw polymers are available, therefore, annealing does not have the same beneficial effect as with P3HT. Optimal conditions for annealing are strongly dependent on the polymer Mw and processing conditions. In the case for P3HT:PCBM, optimal efficiencies were obtained using a combination of annealing before, as well as after contact deposition.

Using the concepts developed for P3HT, the effect of solvent, molecular weight and the type of fullerenes was investigated using MEH-PPV. Using an aromatic solvent with a high molecular weight MEH-PPV contributes to an ordered chain alignment enhancing the devices performance. Annealing was not performed on the devices due preliminary results indicating a rapid reduction in performance with annealing. Considering that annealing increases crystallinity, therefore improve charge mobility, further study should be performed to optimize the annealing conditions. Finally, using the C70 PCBM instead of the C60 PCBM significantly increased the current density but not the Voc. Efficiencies were

increased from 0.57% to 2.06% under AM1.5 by optimizing the polymer molecular weight, the device thickness and the fullerene derivative.

Three types of quantum dots were investigated to enhance photoconversion below the polymer absorption. CdSe QDs were successfully added to MEH-PPV to improve device efficiency. The processing conditions were therefore applied for other systems. Composites of InP QDs and MEH-PPV were not as successful as the CdSe system due to the difficult ligand exchange process. Therefore, InAs QDs were synthesized using a different approach without the problematic myristic acid ligand. Sub-bandgap photoconversion was observed around 1.3 eV but due to the inappropriate energy level alignment of the elements, the performance were lowered by the addition of the QDs. The energy levels of different materials vary considerably in the literature and therefore, it is difficult to predict how a real device will perform by mixing different components.

Finally, both SWNT and WMNT were investigated for improved charge dissociation and transport in organic solar cells. The purified SWNT loading was limited below 0.5%. Two approaches were successfully applied to overcome the possible contact of carbon nanotubes with the electrodes. The maximum loading was increased by using cut carbon nanotubes as well as by using an intrinsic layer. The most promising option for using carbon nanotubes in polymeric solar cells was found to be the MWNT aligned arrays which can improve charge transport.

Appendix

Appendix A: Photovoltaic characterization

Characteristic current-voltage curve for a solar cell is shown in Figure 47. The fourth quadrant is the power quadrant since the device produces power under light.

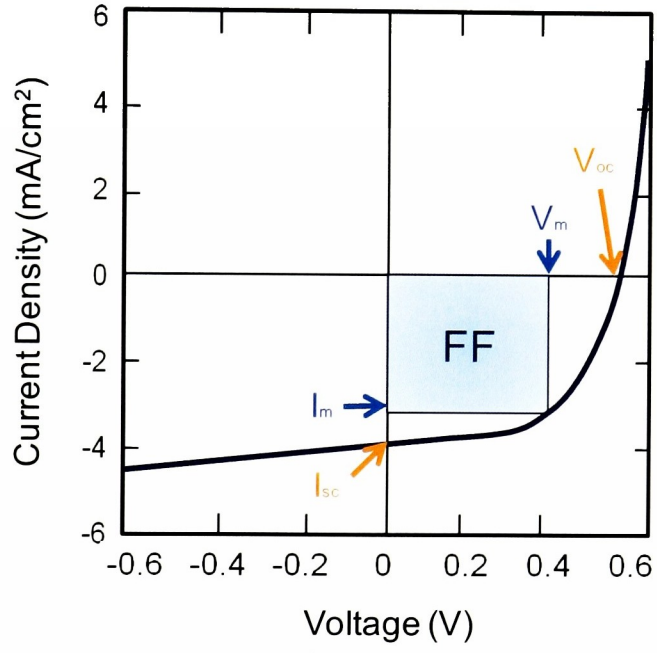

Figure 54: Current-Voltage (I-V) curves for an organic solar cell

The photovoltaic power conversion efficiency of a solar cell is determined by:

$$\eta_e = \frac{V_{oc} * I_{SC} * FF}{P_{in}}$$

For which the FF is defined as:

$$FF = \frac{I_m * V_m}{I_{sc} * V_{oc}}$$

V_{oc} is the open circuit voltage, I_{sc} is the short circuit current, FF is the fill factor and P_{in} is the incident light power density. For the AM1.5 spectrum, the light intensity is standardized at

1000 W/m^2, with a spectral intensity distribution matching that of the sun on the earth's surface at an incident angle of 48.2. For AM0, the light intensity is 1336.1 W/m^2 at a zero angle,[50] as illustrated in the next figure.

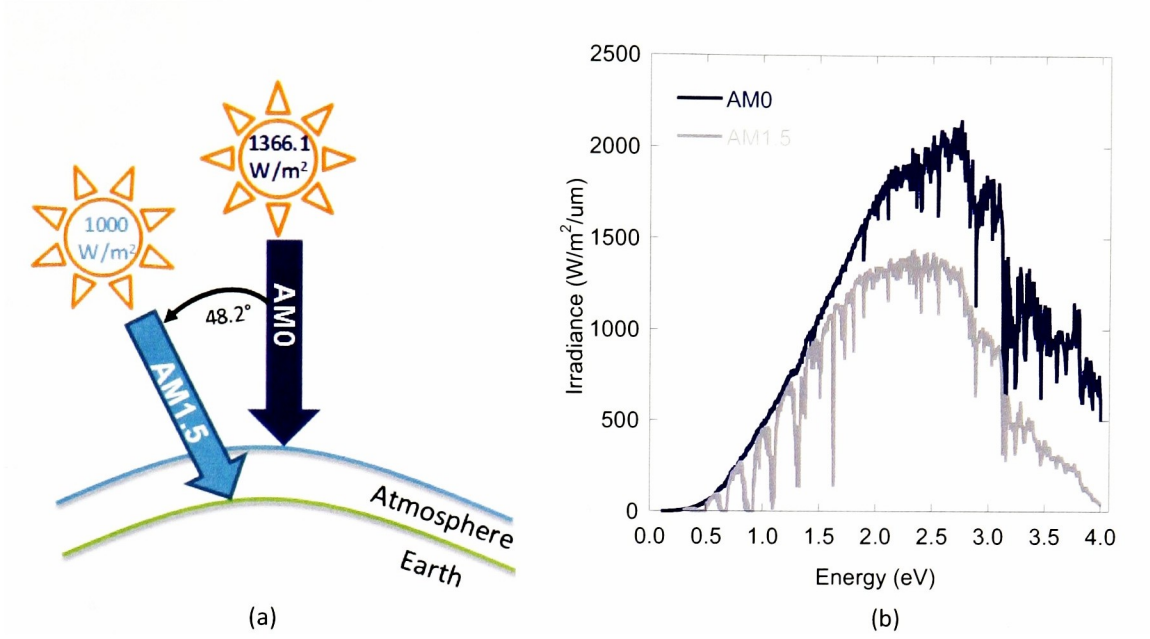

Figure 55: (a) Difference between AM0 and AM1.5[50] and (b) irradiance as a function of energy.

Organic solar cells performance can also be characterized using spectral response to measure the external quantum efficiency which corresponds to the number of electrons collected under short circuit conditions divided by the number of incident photons.[7]

$$E.Q.E = \frac{1240 I_{sc}}{\lambda P_{in}}$$

λ (nm) is the incident photon wavelength, Isc is the photocurrent of the device, and P_{in} is the incident power.

References

1. Tang, C. W., Two-layer organic photovoltaic cell. *Applied Physics Letters* **1986,** 48, (2), 183-185.

2. Yu, G. U. C.; Gao, J.; Hummelen, J. C.; Wudl, F.; Heeger, A. J., Polymer photovoltaic cells: enhanced efficiencies via a network of internal donor-acceptor heterojunctions. *Science* **1995,** 270, (5243), 1789-1791.

3. Ma, W.; Yang, C.; Gong, X.; Lee, K.; Heeger, A. J., Thermally stable efficient polymer solar cells with nanoscale control of the interpenetrating network morphology. *Advanced Functional Materials* **2005,** 15, (10), 1617-1622.

4. Li, G.; Shrotriya, V.; Huang, J.; Yao, Y.; Moriarty, T.; Emery, K.; Yang, Y., High-efficiency solution processable polymer photovoltaic cells by self-organization of polymer blends. *Nature Materials* **2005,** 4, (11), 864-868.

5. Janssen, R. A. J.; Hummelen, J. C.; Sariciftci, N. S., Polymer-fullerene bulk heterojunction solar cells. *MRS Bulletin* **2005,** 30, (1), 33-36.

6. Moliton, A.; Nunzi, J.-M., How to model the behaviour of organic photovoltaic cells. *Polymer International* **2006,** 55, (6), 583-600.

7. Guenes, S.; Neugebauer, H.; Sariciftci, N. S., Conjugated Polymer-Based Organic Solar Cells. *Chemical Reviews (Washington, DC, United States)* **2007,** 107, (4), 1324-1338.

8. El Ela, A. H. A.; Afifi, H. H., Hopping Transport in Organic Semiconductor System. *Journal of Physics and Chemistry of Solids* **1979,** 40, (4), 257-259.

9. Gregg, B. A., The photoconversion mechanism of excitonic solar cells. *MRS Bulletin* **2005,** 30, (1), 20-22.

10. Scharber, M. C.; Muehlbacher, D.; Koppe, M.; Denk, P.; Waldauf, C.; Heeger, A. J.; Brabec, C. J., Design rules for donors in bulk-heterojunction solar cells-towards 10 % energy-conversion efficiency. *Advanced Materials (Weinheim, Germany)* **2006,** 18, (6), 789-794.

11. Schwartz, M., Encyclopedia of Smart Materials. In [Online] Sons, J. W., Ed.

12. Wikipedia Polythiophene. http://en.wikipedia.org/wiki/Polythiophenes

13. Kim, Y.; Cook, S.; Tuladhar, S. M.; Choulis, S. A.; Nelson, J.; Durrant, J. R.; Bradley, D. D. C.; Giles, M.; McCulloch, I.; Ha, C.-S.; Ree, M., A strong regioregularity effect in self-organizing conjugated polymer films and high-efficiency polythiophene:fullerene solar cells. *Nature Materials* **2006,** 5, (3), 197-203.

14. Kim, K.; Liu, J.; Namboothiry, M. A. G.; Carroll, D. L., Roles of donor and acceptor nanodomains in 6% efficient thermally annealed polymer photovoltaics. *Applied Physics Letters* **2007,** 90, (16), 163511/1-163511/3.

15. Padinger, F.; Rittberger, R. S.; Sariciftci, N. S., Effects of postproduction treatment on plastic solar cells. *Advanced Functional Materials* **2003,** 13, (1), 85-88.

16. Pandey, A. K.; Wang, H. e. a., Improved performance of organic nano-composite solar cells with reverse biased annealing. *Nonlinear Optics and Quantum Optics* **2007,** 37, 123-131.

17. Chang, E. C.; Chao, C.-I.; Lee, R.-H., Enhancing the efficiency of MEH-PPV and PCBM based polymer solar cells via optimization of device configuration and processing conditions. *Journal of Applied Polymer Science* **2006,** 101, (3), 1919-1924.

18. Cao, G., *Nanostructures & nanomaterials : synthesis, properties & applications*. London : Imperial College Press: 2004; p 433.

19. Solenne Solenne. http://www.solennebv.com/products

20. Guyot-Sionnest, P., Intraband Spectroscopy and Semiconductor Nanocrystals. *Structure and Bonding (Berlin, Germany)* **2005,** 118, (Semiconductor Nanocrystals and Silicate Nanoparticles), 59-77.

21. Murray, C. B.; Norris, D. J.; Bawendi, M. G., Synthesis and Characterization of Nearly Monodisperse CdE Semiconductor Nanocrystallites. *Journal of American Chemical Society* **1993,** 115, (19), 8706-8715.

22. Peng, X.; Thessing, J., Controlled synthesis of high quality semiconductor nanocrystals. *Structure and Bonding (Berlin, Germany)* **2005,** 118, (Semiconductor Nanocrystals and Silicate Nanoparticles), 79-119.

23. Tang, A.-w.; Teng, F.; Jin, H.; Gao, Y.-h.; Hou, Y.-b.; Liang, C.-j.; Wang, Y.-s., Investigation on photoconductive properties of MEH-PPV/CdSe-nanocrystal nanocomposites. *Materials Letters* **2007,** 61, (11-12), 2178-2181.

24. Choi, S.-H.; Song, H.; Park, I. K.; Yum, J.-H.; Kim, S.-S.; Lee, S.; Sung, Y.-E., Synthesis of size-controlled CdSe quantum dots and characterization of CdSe-conjugated polymer blends for hybrid solar cells. *Journal of Photochemistry and Photobiology, A: Chemistry* **2006,** 179, (1-2), 135-141.

25. Battaglia, D.; Peng, X., Formation of High Quality InP and InAs Nanocrystals in a Noncoordinating Solvent. *Nano Letters* **2002,** 2, (9), 1027-1030.

26. Yu, P.; Zhu, K.; Norman, A. G.; Ferrere, S.; Frank, A. J.; Nozik, A. J., Nanocrystalline TiO2 solar cells sensitized with InAs quantum dots. *Journal of Physical Chemistry B* **2006,** 110, (50), 25451-25454.

27. Rowell, M. W.; Topinka, M. A.; McGehee, M. D.; Prall, H.-J.; Dennler, G.; Sariciftci, N. S.; Hu, L.; Gruner, G., Organic solar cells with carbon nanotube network electrodes. *Applied Physics Letters* **2006,** 88, (23), 233506-233508.

28. Miller, A. J.; Hatton, R. A.; Chen, G. Y.; Silva, S. R. P., Carbon nanotubes grown on In2O3: Sn glass as large area electrodes for organic photovoltaics. *Applied Physics Letters* **2007,** 90, (2), 023105-023107.

29. Hiorns, R. C.; de Bettignies, R.; Leroy, J.; Bailly, S.; Firon, M.; Sentein, C.; Khoukh, A.; Preud'homme, H.; Dagron-Lartigau, C., High molecular weights, polydispersities, and annealing temperatures in the optimization of bulk-heterojunction photovoltaic cells based on poly(3-hexylthiophene) or poly(3-butylthiophene). *Advanced Functional Materials* **2006,** 16, (17), 2263-2273.

30. Landi, B. J.; Raffaelle, R. P.; Castro, S. L.; Bailey, S. G., Single-wall carbon nanotube-polymer solar cells. *Progress in Photovoltaics: Research and Applications* **2005,** 13, (2), 165-172.

31. Savenije, T. J.; Kroeze, J. E.; Yang, X.; Loos, J., The formation of crystalline P3HT fibrils upon annealing of a PCBM:P3HT bulk heterojunction. *Thin Solid Films* **2006,** 511-512, 2-6.

32. Kim, Y.; Choulis, S. A.; Nelson, J.; Bradley, D. D. C.; Cook, S.; Durrant, J. R., Composition and annealing effects in polythiophene/fullerene solar cells. *Journal of Materials Science* **2005,** 40, (6), 1371-1376.

33. Kim, H.; So, W.-W.; Moon, S.-J., The importance of post-annealing process in the device performance of poly(3-hexylthiophene): Methanofullerene polymer solar cell. *Solar Energy Materials and Solar Cells* **2007,** 91, (7), 581-588.

34. Kim, Y.; Choulis, S. A.; Nelson, J.; Bradley, D. D. C.; Cook, S.; Durrant, J. R., Device annealing effect in organic solar cells with blends of regioregular poly(3-hexylthiophene) and soluble fullerene. *Applied Physics Letters* **2005,** 86, (6).

35. Yamanari, T.; Taima, T.; Hara, K.; Saito, K., Investigation of optimum conditions for high-efficiency organic thin-film solar cells based on polymer blends. *Journal of Photochemistry and Photobiology A: Chemistry* **2006,** 182, (3), 269-273.

36. Liu, J.; Shi, Y.; Yang, Y., Solvation-induced morphology effects on the performance of polymer-based photovoltaic devices. *Advanced Funtional Materials* **2001,** 11, (6), 420-424.

37. Koynov, K.; Bahtiar, A.; Ahn, T.; Cordeiro, R. M.; Horhold, H.-H.; Bubeck, C., Molecular weight dependence of chain orientation and optical constants of thin films of the conjugated polymer MEH-PPV. *Macromolecules* **2006,** 39, (25), 8692-8698.

38. Niu, Y.-H.; Hou, Q.; Caoa, Y., Thermal annealing below the glass transition temperature: A general way to increase performance of light-emitting diodes based on copolyfluorenes. *Applied physics letters* 81, (4), 3.

39. Zheng, L.; Zhou, Q.; Deng, X.; Yuan, M.; Yu, G.; Cao, Y., Methanofullerenes used as electron acceptors in polymer photovoltaic devices. *Journal of Physical Chemistry B* **2004,** 108, (32), 11921-11926.

40. Zhang, F. L.; Johansson, M.; Andersson, M. R.; Hummelen, J. C.; Inganas, O., Polymer solar cells based on MEH-PPV and PCBM. *Synthetic Metals* **2003,** 137, (1-3), 1401-1402.

41. Li, J. J.; Wang, Y. A.; Guo, W.; Keay, J. C.; Mishima, T. D.; Johnson, M. B.; Peng, X., Large-scale synthesis of nearly monodisperse CdSe/CdS core/shell nanocrystals using air-stable reagents via successive ion layer adsorption and reaction. *ournal of the American Chemical Society* **2003,** 125, (41), 12567-12575.

42. Becker, G.; Gutekunst, G.; Wessely, H. J., Trimethylsilyl compounds of Vb elements. I. Syntheses and properties of trimethylsilylarsines. *Zeitschrift fuer Anorganische und Allgemeine Chemie* **1980,** 462, 113-29.

43. Guzelian, A. A.; Banin, U.; Kadavanich, A. V.; Peng, X.; Alivisatos, A. P., Colloidal chemical synthesis and characterization of InAs nanocrystal quantum dots. *Applied Physics Letters* **1996,** 69, (10), 1432-1434.

44. Furis, M.; MacRae, D. J.; Lucey, D. W.; Sahoo, Y.; Cartwright, A. N.; Prasad, P. N. In *Spectroscopy studies of InP nanocrystals synthesized through a fast reaction*, Materials Research Society Symposium, 2003; 2003; pp 89-94.

45. Solomeshch, O.; Kigel, A.; Saschiuk, A.; Medvedev, V.; Aharoni, A.; Razin, A.; Eichen, Y.; Banin, U.; Lifshitz, E.; Tessler, N., Optoelectronic properties of polymer-nanocrystal composites active at near-infrared wavelengths. *Journal of Applied Physics* **2005,** 98, (7), 074310/1-074310/6.

46. Thompson, B. C.; Kim, Y.-G.; Reynolds, J. R., Spectral Broadening in MEH-PPV:PCBM-Based Photovoltaic Devices via Blending with a Narrow Band Gap Cyanovinylene-Dioxythiophene Polymer. *Macromolecules* **2005,** 38, (13), 5359-5362.

47. DiLeo, R. A.; Landi, B. J.; Raffaelle, R. P., Purity assessment of multiwalled carbon nanotubes by Raman spectroscopy. *Journal of Applied Physics* **2007,** 101, (6), 064307-064309.

48. Afzali, A.; Dimitrakopoulos, C. D.; Breen, T. L., High-performance, solution-processed organic thin film transistors from a novel pentacene precursor. *Journal of the American Chemical Society* **2002,** 124, (30), 8812-8813.

49. Kang, S. J.; Yi, Y.; Kim, C. Y.; Cho, S. W.; Noh, M.; Jeong, K.; Whang, C. N., Energy level diagrams of C60/pentacene/Au and pentacene/C 60/Au. *Synthetic Metals* **2006,** 156, (1), 32-37.

50. Rostalski, J.; Meissner, D., Monochromatic versus solar efficiencies of organic solar cells. *Solar Energy Materials and Solar Cells* **2000,** 61, (1), 87-95.